Local Calibration Review of AASHTOWare Flexible Pavement Mechanistic Empirical Design Software for Kansas

by

Noura Sultan Hassan Mahmoud Saleh

MSc., Louisiana State University, 2020

A REPORT

submitted in partial fulfillment of the requirements for the degree

MASTER OF SCIENCE

Department of Civil Engineering
Carl. R. Ice College of Engineering

KANSAS STATE UNIVERSITY
Manhattan, Kansas

2023

Approved by:
Major Professor
Dr. Parth Panchmatia

Copyright

Abstract

Multiple state highway authorities have been pursuing the adoption of the latest AASHTOWare Pavement Mechanistic-Empirical Design (PMED). The PMED design guide utilizes theories of mechanics to predict pavement stress and strain responses using transfer functions to convert these responses to pavement distresses. These functions must be calibrated to local conditions for an accurate pavement performance prediction and subsequent design analysis. Previously, there were some efforts on local calibration of flexible pavement distress models in Kansas using AASHTOWare PMED versions 2.2.0 and 2.5.0 However, these calibration factors should be checked over time in accordance with updated software versions.

The local calibration factors were evaluated using the newest version of AASHTOWare 2.6.2.2 Twenty-one actual constructed flexible pavements were selected for reviewing the local calibration factors for different distress models, including rutting, fatigue cracking, transverse cracking, and international roughness index (IRI). Statistical analysis was done for all the distresses to check the validity of these calibration factors on the latest AASHTOWare version 2.6.2.2. The new version showed a successful response using global and local calibration factors for rutting distress and IRI. However, top-down fatigue cracking distress function was drastically changed in PMED version 2.6.2.2 and new parameter inputs have been added to the model.

Table of Contents

List of Figures

List of Tables

Acknowledgements

I would like to express my deepest gratitude to Dr. Christopher A. Jones for his support and giving me the chance to finish this chapter of my academic journey.

I extend my heartfelt thanks to my supervisor Dr. Parth Panchmatia for his support, guidance, and his continuous motivation.

I would like to thank Dr. Weston Koehn for his support and efforts during the courses and teaching duties.

I am indebted to my family for their unwavering encouragement and constant belief in my potential. Their love and support have been my greatest motivation.

I want to deeply thank my husband Ahmed Elshoura for his support and love. Additionally, I want to thank my son Younis Elsoura; for always being the main motivation to work hard so he can be proud of his parents.

I sincerely want to thank Trisha Brown, Rebecca Darkow, Clifford Temple, and Melissa Pierce for all their help, patience, and generosity.

I am also very thankful to my graduate colleagues for their support and encouragement.

Introduction

The pavement design guide by the American Association of State Highway and Transportation Officials (AASHTO) has been predominantly used by the state highway agencies in the United States (AASHTO 1993). The AASHTO methodology is empirical in nature and developed from the AASHO Road Test results (Huang 1993). However, an update was necessary to integrate the fundamental principles of engineering mechanics into the process of pavement design (Khanum, 2005). While the 1993 AASHTO design guide is widely recognized as a pavement design standard, there was a need for an update to integrate engineering mechanics principles into pavement design (Khanum, 2005). To address the limitations of the 1993 AASHTO design guide, an innovative mechanistic-empirical pavement design guide (MEPDG) was produced. The development of the MEPDG method was carried out within the framework of the National Cooperative Highway Research Program (NCHRP) 1-37A project. This advanced approach considers various crucial input parameters, such as traffic conditions, climate factors, and pavement material properties. The MEPDG design guide leverages principles of mechanics to evaluate pavement performance. It can accomplish this by predicting pavement stress and strain responses while calculating incremental damage accumulation over time (Li et al., 2011; Robbins, 2017). To convert cumulative damage into pavement distress assessments, transfer functions are typically employed. These functions undergo empirical calibration using real distress data from in-service pavement sections.

The MEPDG incorporated its design approach in a software, known as AASHTOWare Pavement ME design (PMED) version 1.1. Over time, AASHTOWare underwent several improvements until the latest version 2.6.0. PMED transfer functions were globally calibrated based on Long-Term Pavement Program (LTPP) database, as reported by (Li et. al, 2011).

Although the PMED AASHTOWare predicts the performance of a new or rehabilitated pavement design based on global calibration factors, it may not give an accurate prediction of distresses for an identical state or region. Due to variations in design, construction practices, traffic, climate, and material conditions among different states, the prediction models in PMED must undergo a state-specific or regional calibration process. Calibration process involves minimizing the bias, residual error, and standard error between the actual pavement distress values (observed) and those predicted values from the AASHTOWare (Kim et. al, 2011). The calibration and validation process for every performance model to the local condition has been described in detail by Nantung et. al (2005).

The Kansas Department of Transportation (KDOT) is in the process of shifting from the utilization of the 1993 AASHTO Pavement Design Guide to the adoption and implementation of PMED. Previously, efforts were undertaken for flexible pavement local calibration of performance models for the state of Kansas. The first local calibration was done for in-service flexible pavements using the AASHTOWare version 2.2.0 (Abusufian, 2015). Then, the process was repeated for new rehabilitated projects using AASHTOWare version 2.5 (Islam, 2019). Local calibration was carried out for permanent deformation or rutting, top-down fatigue cracking, transverse cracking, and IRI distress models for the flexible pavements.

One of the most challenging issues for implementing the PMED software is the need of periodic calibration with updated performance data (Islam, 2019). Since the latest version of AASHTOWare PMED is 2.6.2.2, the calibration factors of performance models need to be tested globally, and locally for Kansas. The main objective of this study is to find the distresses response of pavements in-service using the global and local calibration factors in AASHTOWare. Then, evaluating the results based on bias, residuals, and standard error between the measured and predicted distresses. Eventually, deciding if the local calibration factors that were previously implemented still valid to be used in upcoming flexible pavement design in Kansas.

Literature Review

This chapter introduces the distress prediction models used by the Mechanistic Empirical Pavement Design Guide (MEPDG). It provides a brief description of AASHTOWare software. It also covers the hierarchical tiers of input commonly employed in AASHTOWare's pavement ME design software.

Definition of MEPDG

MEPDG represents a pavement design approach firmly rooted in mechanistic principles. It encompasses critical factors intricately linked to pavement performance, including traffic loads, climatic influences, material characteristics, and the existing soil condition (NCHRP, 2014). As its name implies, this design methodology consists of two distinct components for analysis and design: the mechanistic aspect and the empirical aspect. The mechanistic part relies on fundamental physics to estimate how the pavement reacts to factors such as wheel loads or environmental conditions, evaluating parameters like stress, strain, and displacement. In contrast, the empirical element utilizes the calculated pavement response to forecast the pavement's longevity based on real-world field performance (Timm et al., 1988).

Superiority of Mechanistic-Empirical (ME) over Empirical Design

The Mechanistic-Empirical (ME) method offers several distinct advantages over traditional Empirical Design Procedures (EDPs), signifying a significant advancement in pavement design practices. Some of these advantages are outlined below, with references to FHWA (2014) and other relevant sources:

- Customization and Adaptability: One of the primary advantages of the ME method is its adaptability. ME designs can be tailored to specific project conditions, considering factors like traffic loadings, climate, material properties, and local soil conditions (FHWA, 2014).

This customization ensures that pavement designs are better suited to the unique characteristics of a given location.

- Mechanistic Foundation: The ME method is grounded in the principles of engineering mechanics. It explicitly considers the structural responses of pavements to applied loads, including stress, strain, and deflection (FHWA, 2014). This mechanistic foundation leads to more accurate predictions of pavement performance.
- Improved Reliability: By integrating both mechanistic and empirical aspects, the ME method provides a more reliable means of predicting pavement performance and life. It considers a broader range of factors that affect performance and reliability, ultimately leading to more robust pavement designs (FHWA, 2014).
- Increased Performance Life: ME designs are better equipped to extend the life of pavements. By accurately modeling how materials and structures will perform under various conditions, the ME method can help design pavements that are more durable and require fewer repairs over time.
- Cost-Effective Solutions: Through its mechanistic approach, the ME method can identify the most cost-effective design strategies. This capability is vital for transportation agencies looking to maximize their investments in pavement infrastructure (FHWA, 2014).
- Prediction of Distresses: ME designs not only focus on the thickness of pavement but also predict the performance of the pavement over its design life. This prediction includes the potential distresses the pavement may encounter (Timm et al., 1988).
- Improved Understanding: The ME method enhances the understanding of the complex interactions between traffic, materials, climate, pavement structure, and construction

parameters. This deep understanding allows for more informed decision-making in pavement design (FHWA, 2014).

Mechanistic-Empirical method stands out as a superior approach to pavement design when compared to traditional Empirical Design Procedures. It leverages a mechanistic foundation to provide more accurate, reliable, and customized pavement solutions. With a focus on performance, durability, and cost-effectiveness, the ME method represents a significant advancement in the field of pavement engineering.

Design Principals of MEPD

The Mechanistic-Empirical (ME) pavement design method, outlined in NHI (2002) and supported by additional references, is characterized by a set of key principles that guide its application. These principles are integral to understanding the ME approach and include inputs, structural response modeling, performance prediction models, performance criteria, and design reliability.

1. Inputs: The ME design method begins with the collection of comprehensive input data. These inputs encompass the pavement structure, materials, traffic loads, climate conditions, and soil properties (NHI, 2002). The accuracy of these data is essential to the reliability of the subsequent design process (FHWA, 2014).
2. Structural Response Model: A fundamental aspect of the ME method is its reliance on mechanics. It employs structural response models to estimate critical pavement responses, such as stress, strain, and deflection (FHWA, 2014). This mechanistic approach allows for a more rigorous analysis of pavement behavior.
3. Performance Prediction Models: The ME method integrates performance prediction models to anticipate how pavements will perform over their design life (NHI, 2002). These

models are based on empirical relationships that link pavement distress and performance with various input parameters (FHWA, 2014). By considering a range of factors, the ME method enables a more thorough evaluation of pavement performance.

4. Performance Criteria: ME design relies on predetermined performance criteria that serve as a main reference for evaluating pavement performance (NHI, 2002). These criteria typically relate to various distresses and performance indicators, such as cracking, rutting, and smoothness. The chosen criteria play a significant role in assessing the adequacy of the pavement design (FHWA, 2014).
5. Design Reliability: Design reliability refers to the level of certainty with which pavement performance can be predicted. The ME method allows users to specify the desired level of design reliability (NHI, 2002). It accounts for variability in inputs and evaluates the associated uncertainties in performance predictions. This aspect is particularly important in addressing the inherent uncertainty in the design process (FHWA, 2014).

These principles collectively define the core of the ME pavement design method. They underline the significance of reliable input data, the application of mechanistic structural models, the use of performance prediction models to anticipate distresses and performance outcomes, the establishment of performance criteria, and the consideration of design reliability in accounting for variability.

Background About AASHTOWare

The AASHTOWare pavement design software is a comprehensive suite of tools that plays a vital role in the field of civil engineering, particularly in the design and analysis of pavements. Developed by AASHTO, this software is widely regarded as a state-of-the-art solution for pavement design. It incorporates the latest principles of engineering mechanics and employs a mechanistic-empirical (ME) approach, allowing engineers to design pavements that not only meet but exceed performance expectations.

The core principles of AASHTOWare pavement design software include consideration of various factors that influence pavement performance. These factors range from traffic loadings and climatic effects to material properties and existing soil conditions (AASHTO, 2010). The software's mechanistic component enables the estimation of pavement responses to wheel loads and environmental conditions in terms of stress, strain, and displacement. These responses are then integrated into the empirical portion of the design, which leverages computed pavement responses to predict the pavement's life based on real-world field performance (Timm et al., 1988). Figure 1 shows a layout of how the flexible pavement scheme works.

One of the standout features of AASHTOWare is its adaptability and flexibility. Designers can incorporate agency-established performance criteria and easily adjust to newer materials and evolving conditions. It allows for a comprehensive understanding of the intricate interactions between traffic, materials, climate, pavement structure, and construction parameters. Moreover, it can evaluate additional damage caused by unique truck loading configurations or increased truck weights, ensuring that pavement designs are robust and resilient (NCHRP, 2014).

The benefits of using AASHTOWare pavement design software are manifold. Designers are not confined to thickness-based design; instead, they have the freedom to control various design features. This includes pavement structure, materials, climatic conditions, season, soil conditions, and traffic loading, which all contribute to creating customized, high-performance pavement solutions. The software also assists in determining the most cost-effective design strategies, and its output can be effectively used in life cycle cost analysis.

The AASHTOware pavement ME design software was developed in accordance with the principles and methodologies outlined in the Mechanistic-Empirical Pavement Design Guide (MEPDG). It consists of a series of modules designed to facilitate the analysis process for pavement designers. This software serves as an interface for inputting design parameters, houses computational engines for mechanistic analysis and performance prediction, and provides results and outputs in a convenient electronic format (NCHRP, 2004). The AASHTOware pavement ME design software encompasses various tools, each with its specific purpose and functionality (AASHTO, 2014) as follows:

- General Design Inputs: involves essential information such as pavement design type, pavement type, design life, and the anticipated construction and opening dates.
- Performance Criteria: the design authority who can define the threshold values for performance prediction models and specify the desired level of reliability.
- Traffic: The traffic assists in determining the loads imposed on the pavement structure. traffic data can be derived from sources like weigh-in-motion (WIM) sites, automatic vehicle classification (AVC) sites, or national defaults.
- Climate: Climate inputs are essential for evaluating the environmental impact on material behavior and pavement performance. The software incorporates data from various U.S. weather stations or using LTPP that can create a virtual climate locations information from nearby climatic stations.
- Asphalt Layer Design Properties: This section includes parameters such as Poisson ratio, density, fatigue endurance limit (if applicable), and interface friction.

- Pavement Structure: enables designers to input comprehensive information about pavement layers, including material types, mix properties, mechanical characteristics, strength properties, thermal properties, and layer thickness.
- Calibration Factors: Designers have the freedom to specify calibration coefficients for performance prediction models. These coefficients can be nationally calibrated at the program level or customized for project-specific requirements.
- Reports: The software offers comprehensive reporting capabilities, allowing users to generate PDF reports and Microsoft Excel files summarizing input details, traffic predictions, climatic information, material properties, and other design-related tables and charts.

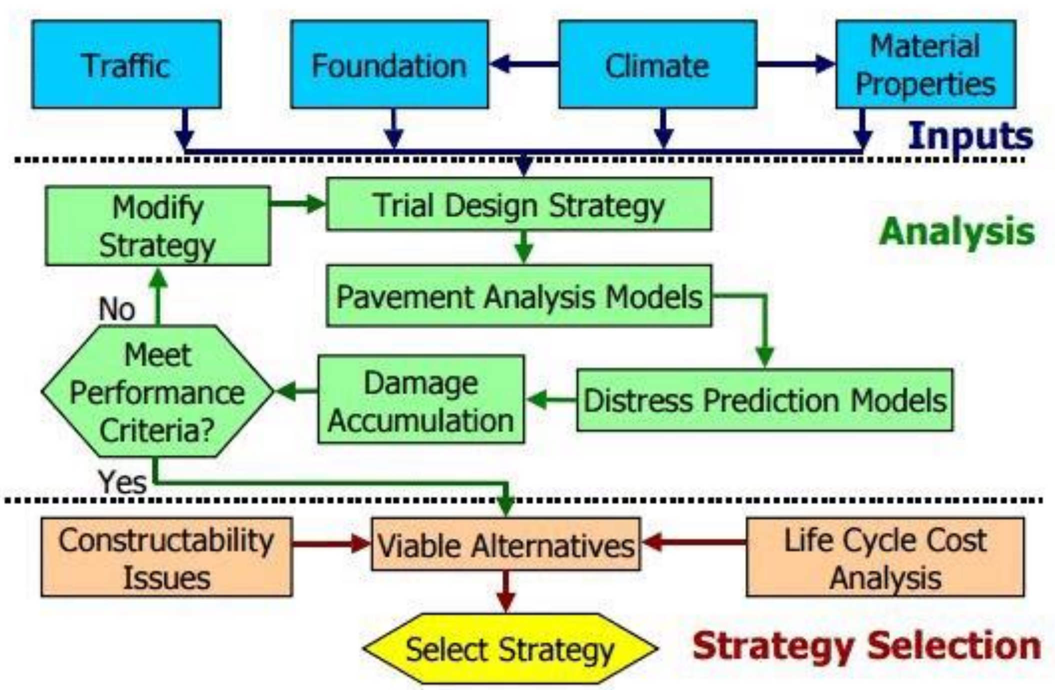

Figure 1. Overview of flexible pavement design (NCHRP, 2004)

Distress Models Calibration Factors

Permanent Deformation/Rutting Model

AASHTOWare Pavement ME Design software uses the incremental damage approach in predicting total rutting. Rutting is estimated as the summation of rut depths accumulated in all bound and unbound layers. The software assumes that no rutting occurs in the stabilized base and sub-base layers (Kim et al. 2011). For HMA mixtures, the permanent deformation model is shown in Equation 1.

$$\Delta_{p(HMA)} = \varepsilon_{p(HMA)} h_{(HMA)} = \beta_{1r} k_z \epsilon_{r(HMA)} 10^{k1r} n^{k2r\beta 2r} T^{k3r\beta r3} \quad (1)$$

Where:

$\Delta p_{(HMA)}$ = Accumulated permanent or plastic vertical deformation in the HMA layer (in)

$\varepsilon_{p(HMA)}$ = Accumulated permanent or plastic axial strain in HMA layer/sublayer (in/in)

$h_{(HMA)}$ = Thickness of the HMA layer/sublayer (in)

$\epsilon_{r(HMA)}$ = Resilient or elastic strain calculated by the structural response model at the mid-depth of each HMA layer (in)

n = Number of axle-load repetitions

T = Mix or pavement temperature (°F)

k_z= Depth confinement factor

"k_{1r}", "k_{2r}", "k_{3r}" = Global calibration factors (material specific coefficients that are determined from the repeated load tri-axial tests for permanent deformation)

β"$_{1r}$", β"$_{2r}$", β"$_{3r}$" = calibration coefficients

For unbound layers, the rut depth model is shown in equation 2.

$$\Delta_{p(soil)} = \beta_{s1} k_{s1} \epsilon_v h_{soil} \left(\frac{\epsilon_o}{\epsilon_r}\right) e^{-\left(\frac{\rho}{n}\right)^{\beta}} \quad (2)$$

Where:

$\Delta_{p(soil)}$ = Permanent or plastic vertical deformation in the unbound layer (in)

ϵ_o = determined from laboratory repeated load permanent deformation tests (in/in)

ϵ_r = Resilient strain imposed in laboratory test to obtain material properties (in/in)

ϵ_v = Average vertical resilient or elastic strain in the unbound layer calculated by the structural response model (in/in)

h_{soil} = Thickness of the unbound layer (in)

k_{s1} = Global calibration coefficients

β_{s1} = Local calibration coefficient

The default/global calibration factors of the rutting have changed from AASHTOWare version 5.2.0. to version 2.6.2.2. This will reflect a change in the rutting distress values using the default calibration factors. This finally will affect the calibration process.

IRI Distress Model

AASHTOWare Pavement ME Design software predicts International Roughness Index (IRI) based on equation 3.

$$IRI = IRI_0 + C_1(RD) + C_2(FC) + C_3(TC) + C_4(SF) \tag{3}$$

Where:

IRI = Predicted IRI (in/mile)

IRI_o = Initial IRI after construction (in/mile)

RD = Average rut depth (in)

FC = Area of fatigue cracking (percent total lane area)

TC = Length of transverse cracking (ft/mile)

SF = Site factor (calculated in Equation 4)

C1, C2, C3 = Calibration Factors

$$SF = AGE^{1.5}\{[\ln(P+1)(FI+1)_{P02}]\} + \{[\ln(P+1)(PI+1)_{P200}]\} \tag{4}$$

Where:

AGE = Pavement age (year)

PI = Percent plasticity index of the soil.

P = Average annual precipitation (in)

FI = Average annual freezing index (^{o}F-days)

P02 = Percent passing the 0.02 mm sieve

P200 = Percent passing the 0.075 mm sieve

Top-down Fatigue Cracking Model

A mechanistic-empirical top-down cracking model has been developed in project NCHRP Project 01-52, and the new equation has been approved and released into AASHTOWare PMED version 2.6.0 in 2020. However, the distress model has not been released in the latest edition of the PMED guide. To develop this distress model, new inputs and outputs have been added to the software. Asphalt content by weight and gradation parameter have been added to the updated version as new inputs (NCHRP 2018).

Crack depth and area of cracking over time are new outputs parameters for this version to build the new distress model equation. The project has synthesized and developed multiple components to improve the distress response model. One of the essential implementations for this new model is using the Finite Element Method (FEM) and Artificial Neural Network (ANN) models for computing crack initiation and propagation due to traffic and thermal loading. These new implementations changed the output of the top-down fatigue cracking to be produced as a percentage of lane area instead of a longitudinal crack measured in feet per mile. The Area of top-down cracking in terms of total percent lane area is calculated using a sigmoidal function as shown in Equation 5.

$$L(t) = L_{MaX} e^{-\left(\frac{C1\rho}{t-C3\mathrm{t0}}\right)^{C2\beta}} \tag{5}$$

Where:

L_{Max} = Maximum area of top-down cracking (percent)

t = Analysis month (days)

t_0 = Time to crack initiation (days)

C1, C2, C3 = Calibration coefficients.

ρ and β = Scaling shape parameter.

Time to crack initiation t_0 (days) is calculated based in Equation 6.

$$t_0 = \frac{kL1}{1 + \mathrm{e}^{kL2\;100\left(\frac{a0}{2A0}\right)+KL3(HT)+KL4(LT)+KL5(Log10AADTT)}} \tag{6}$$

Where:

$a_0/2A_0$ = Energy parameters

HT = Annual number of days above 32ºC

LT = Annual number of days below 0ºC

K_{L1}, K_{L2}, K_{L3}, K_{L4}, K_{L5} = Calibration coefficients

$a_0/2A_0 = 0.1796 + 1.5x10^{-5}E_1 - 0.69m - 7.169x10^{-4}Ha$

E1, m= Relaxation modulus power law function parameters for aged asphalt

Ha = Total asphalt layer thickness

Transverse Cracking Model

AASHTOWare MEPDG thermal cracking predicted model is introduced in Equation 7.

$$\Delta \mathrm{C} = \mathrm{A}\,(\Delta K)^n \tag{7}$$

Where:

ΔC = change in crack depth due to a cooling cycle

ΔK = change in the stress intensity factor due to a cooling cycle

A.n = fracture parameters for the HMA mixture

Reasonable estimates of A and n can be derived from the indirect tensile creep compliance and strength of the HMA in accordance with the following two mathematical Equations 8, and 9.

$$A = K_t \beta_t 10^{[4.389 - 2.52\log(E_{HMA}\sigma_m \eta)]} \quad (8)$$

$$\eta = 0.8\left[1 + \frac{1}{m}\right] \quad (9)$$

Where:

K_t = coefficient determined by global calibration for each input level (Level 1 = 1.5; Level 2 = 0.5; and Level 3 = 1.5)

E_{HMA} = HMA indirect tensile modulus (psi)

σ_m = mixture tensile strength (psi)

m = the m-value derived from the indirect tensile creep compliance curve

β_t = local or mixture calibration factor

AASHTOWare Flexible Design Inputs

The AASHTOWare pavement ME design software incorporates a hierarchical approach to input parameters, allowing designers to adapt their design to their knowledge and specific project requirements. The inputs for a new pavement design fall into three main categories: traffic, climate, and material properties. Each category comprises subcategories that offer flexibility for designers to adjust input parameters, aiming to achieve desired distress predictions and reliability (Kasperick, 2013). The software supports three hierarchical input levels, each suitable for assigning material and traffic input values, with varying degrees of specificity:

- Input Level 1: At this level, input parameters are directly measured, requiring site-specific or project-specific data. Traffic inputs, such as average annual daily truck traffic (AADTT), and truck lane usage necessitate detailed data collection. Material inputs require laboratory or field-testing data, such as dynamic modulus (E), or falling weight deflectometer (FWD) deflection testing. Level 1 input involves substantial resources and time and is typically employed for designing pavements with heavy traffic or unique site conditions.

- Input Level 2: Input parameters at this level are user-selected and can be estimated through a more limited testing program or derived from correlations and regression equations. Examples include estimating the average axle group per vehicle and assigning it to a wide number of projects. Designers pick Level 2 when extensive testing or resources are not available.
- Input Level 3: level 3 is typically utilized for designing low-volume roads, where specific project-related data may be limited. The designer might pick the default value, for example the asphalt concrete unit weight is 140pcf as a default number in AASHTOWare.

The AASHTOWare pavement ME design software's hierarchical input system accommodates a range of design scenarios, from highly detailed and data-intensive projects to those with more generalized or default parameter settings. Designers can choose the appropriate input level based on their project's needs and available resources. Figure 2 shows a layout of ASHTOWAre.

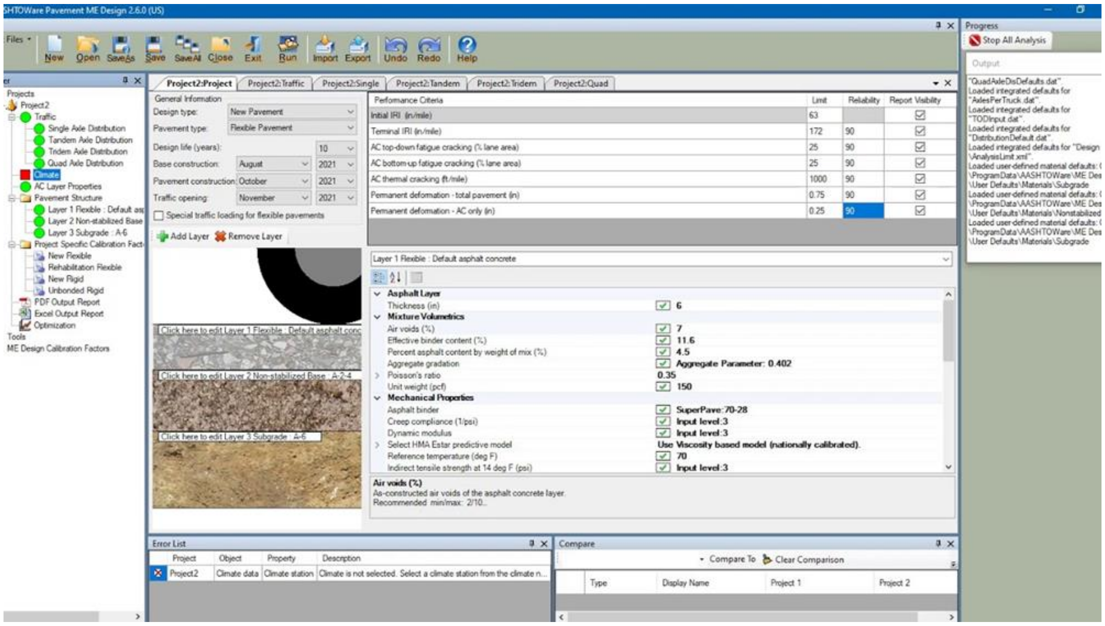

Figure 2. Layout of AASHTOWare Software

Traffic Inputs

Traffic inputs within the AASHTOWare pavement ME design software predominantly rely on the characteristics of truck traffic to represent main factors in the structural design and analysis of pavement systems. Here's a concise overview of the essential traffic inputs necessary for conducting a comprehensive analysis:

- Base Year Truck Volume and Speed: This group of inputs encompasses vital information, including the AADTT for the base year in both directions, lanes numbers in the design direction, trucks percentage in the design lane and lane direction, and the operational speed measured in kilometers per hour (kph).
- Traffic Capacity Cap: This control function enables designers to establish an upper threshold on the estimated traffic volumes utilized in the design process, thereby avoiding the overstepping of the projected highway capacity. Mandatory inputs include AADT, excluding trucks, the growth rate of non-truck linear traffic, the type of highway

facility, the existence of traffic signals, the nature of highway terrain (rural or urban), the capacity limit, and the enforced highway capacity limit.

- Axle Configuration: Several critical inputs comprise the average axle width, quantified in meters (m)
- Lateral Wander: Designers have the capability to define values for parameters like mean wheel location, measured in millimeters (mm), the standard deviation of traffic wander, expressed in millimeters (mm), and the width of the design lane, quantified in meters (m).
- Wheelbase: Input choices include factors such as the mean separation between short axles in meters (m), the typical gap between medium axles in meters (m), the standard spacing of long axles in meters (m), in addition to the proportions of trucks equipped with short, medium, and long axles.
- Vehicle Class Distribution and Growth: This input signifies the standardized allocation of diverse truck classes within the traffic flow, guaranteeing that the cumulative sum of incremental values for all truck categories equals 100%.
- Monthly Distribution Factors: These elements delineate the dispersion of monthly truck volumes over a standard year, with the condition that the total of all monthly distribution factors for a particular truck class equals 12.
- Axle Load Spectra: The term refers to a histogram or distribution of axle loads corresponding to a specific axle type (single, tandem, tridem, or quad) and vehicle class (ranging from class 4 to class 13) According to Figure 3.

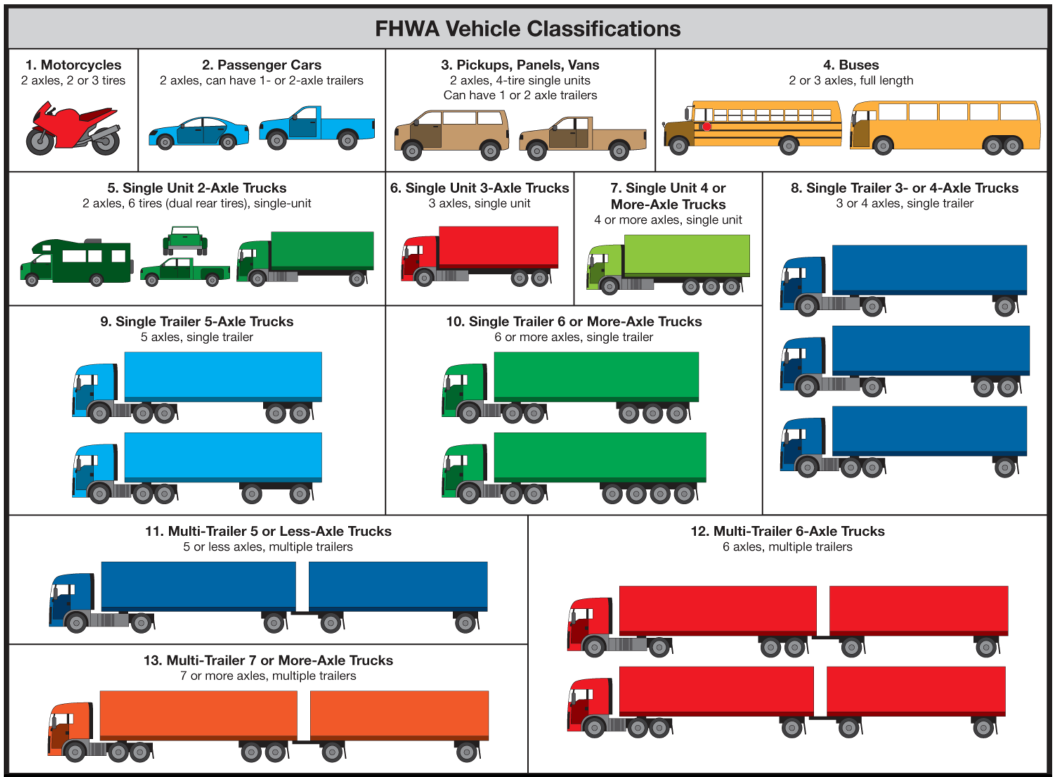

Figure 3. FHWA Vehicle Classifications (Traffic Recorder Instruction Manual 2012)

Climatic Inputs

The performance of flexible pavement is significantly influenced by various environmental factors, including but not limited to precipitation, temperature variations, freeze-thaw cycles, and the depth of the water table. These environmental conditions have a direct impact on the temperature and moisture levels of unbound materials, consequently influencing the pavement's load-carrying capacity. Moreover, temperature levels and gradients play a vital role in determining the stiffness of asphaltic materials. To make accurate predictions about the impact of these environmental factors on pavement performance, the AASHTOWare pavement ME design necessitates the local calibration of these inputs. This calibration process is facilitated through the utilization of an embedded modeling tool known as the enhanced integrated climate (EICM) model. The AASHTOWare pavement ME design software retrieves climate data from weather stations located throughout the United States. These weather stations are commonly found at airports and airfields. The essential inputs obtained from these weather stations include:

- Latitude: The precise latitude of a location, represented in decimal degrees.
- Longitude: The exact longitude of a location, similarly, expressed in decimal degrees.
- Elevation: This input signifies the specific elevation of the project site. It is of utmost importance in determining the lapse rate, which governs how temperature changes with variations in elevation.
- Depth of Water Table: This parameter represents the annual or seasonal average depth of the groundwater table, usually measured from the subgrade's top surface to the groundwater table.
- Climate Station: it implies the selection of a specific weather station for a project site. This might be the exact location of the project or creating a prediction of weather station using data from multiple weather stations near the project (LTTP) database.

Material Inputs

AASHTOWare defines the flexible pavement classification based on the asphalt concrete type including HMA, dense and open-graded asphalt, Asphalt-stabilized base mixes, cold-mix asphalt, central-plant processed, and cold in-place recycled.

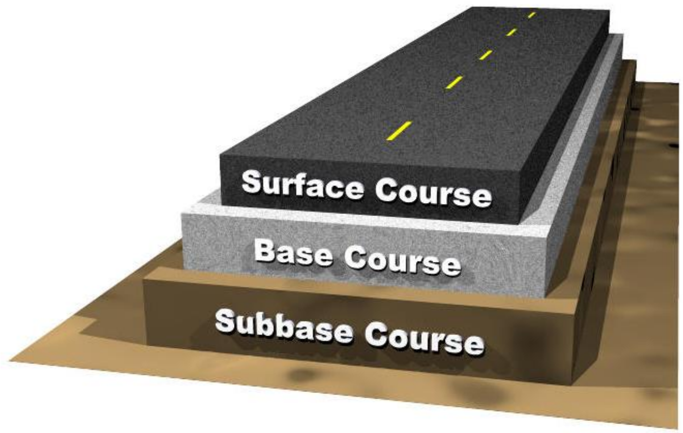

Figure 4. Asphalt Pavement Layers (Kou et. al, 2017)

The surface asphalt layer should have a base layer underneath it to carry the load with the asphalt as shown in Figure 4. This layer should be crushed aggregate, or soil stabilized using different methods including cement stabilized open-graded, cement stabilized, soil cement, lime-cement-fly ash, or lime-treated materials (AASHTO, 2014). AASHTOWare provides the ability for designers to insert the mechanical properties of these materials including layer thickness, unit weight, Poisson's ratio, resilient modulus, modulus of rupture, thermal conductivity, and heat capacity.

Eventually, the subgrade layer is the last layer of the flexible pavement as shown in Figure 4 the subgrade layer is the natural soil layer. In Kansas, 12-in layer is being compacted from the original soil to reduce the elasticity and improve the density.

Local Calibration of MEPDG Process

The local calibration process involves a series of steps, including the collection of field data, performance modeling, and iterative adjustments to model parameters. Field data collection entails the gathering of information on factors such as material properties, traffic loads, climate data, and distress observations. This data serves as the foundation for the calibration process.

Performance modeling is the core of the calibration process, where the collected data is integrated into the mechanistic-empirical models. The software uses this data to make predictions about distresses, such as cracking, rutting, and faulting, over the pavement's design life. The predicted distresses are then compared to actual observations from the field.

Iterative adjustments are made to model parameters based on the disparities between predicted and observed distresses. By fine-tuning these parameters, the software can better reflect the actual conditions of the project site. This calibration process continues until a specified standard error by AASHTO is met of accuracy is achieved, aligning the software's predictions with real-world performance.

The benefits of local calibration are manifold. It enables designers to account for the influence of regional variations in climate, materials, and traffic patterns. Consequently, this process results in more accurate and reliable pavement designs that are better equipped to handle the specific challenges of the local environment.

Incorporating local calibration in the pavement design process promotes cost-effective and sustainable infrastructure. By tailoring designs to local conditions, it reduces the risk of premature pavement failures, minimizes maintenance costs, and extends the service life of the pavement. As a result, local calibration not only enhances the safety and performance of roadways but also contributes to the efficient allocation of resources in the transportation sector.

Methodology

This study was implemented to evaluate the distress models when applying the global and local calibration factors on the latest version 2.6.2.2. Additionally find out if further calibration process is needed. Twenty-seven newly constructed flexible pavement projects were selected for the study. Twenty-one pavement projects were selected for the distresses evaluation and six projects were used for validation. The projects data inputs (material properties, traffic, projects coordinates) were collected from the KDOT database. The levels of projects data input were selected based on the data availability. The design analysis was done for the twenty-one projects using the default calibration factors, then using the local calibration factors. The performance models were checked based on the KDOT failure criteria. Statistical t-test was done to find the linear relation between actual and predicted distress results using default and local calibration factors. Table 1, 2 and Appendix A1 show the projects used for evaluating the local calibration.

Materials Input Parameters

Asphalt Concrete (AC) Layer Properties

The dynamic modulus (E*), the creep compliance, the dynamic shear modulus (G*), the phase angle (δ) of the asphalt binder, and the direct tensile strength of the Hot-Mix-Asphalt (HMA) are required as level 1 inputs for the AASHTOWare PMED. Since all the stated material inputs were not available for the selected projects, level 3/default data inputs were applied. Asphalt mixes volumetric properties, binder grade, and aggregate gradation were extracted from the KDOT mix design database for the surface, intermediate, and base AC layers. The Poisson's ratio of the HMA was taken as 0.35, and the HMA unit weight was taken to be 140 pcf (2,243 kg/m3). The air voids in the surface course mix and the base course mix were 7%. Data inputs (aggregate gradation, binder grade and mix volumetric properties) for all the projects are listed in Appendix A2.

Table 1. Selected projects of flexible pavement for local calibration check

No.	Project Name	Route	County	Begin milepost	End milepost	Length (mile)
1	007U0007500-NB	US-75	Brown	13.05	19.68	6.63
2	008U0005400-EB	US-54	Butler	17.47	25.69	8.22
3	008U0007700-NB-1	US-77	Butler	0.00	12.71	12.71
4	008U0007700-NB-2	US-77	Butler	33.88	43.44	9.56
5	008U0007700-NB-3	US-77	Butler	43.44	50.67	7.23
6	011U0006900-NB	US-69	Cherokee	8.45	11.44	2.99
7	019K0000700-NB-1	K-7	Crawford	0.00	4.97	4.97
8	019K0000700-NB-2	K-7	Crawford	4.97	10.99	6.02
9	019U0016000-EB	US-160	Crawford	9.69	14.54	4.85
10	023U0004000-EB	US-40	Douglas	11.24	12.44	1.20
11	025K0009900-NB	K-99	Elk	12.92	21.72	8.80
12	027K0015600-EB	K-156	Ellsworth	5.63	18.40	12.77
13	028U0005000-EB	US-50	Finney	19.88	29.37	9.48
14	031K0001800-WB	K-18	Geary	15.55	17.55	2.00
15	033U0028300-NB	US-283	Graham	16.96	30.36	13.40
16	052U0007300-NB	US-73	Leavenworth	18.45	20.92	2.47
17	065K0002700-NB	K-27	Morton	0.00	2.67	2.67
18	065U0005600-EB	US-56	Morton	19.76	21.87	2.12
19	069U0028300-NB	US-283	Norton	21.55	32.05	10.50
20	082U0018300-NB	US-183	Rooks	0.00	5.92	5.92
21	095U0005600-EB	US-56	Stevens	8.57	11.12	2.55

Table 2. Selected projects of flexible pavement for validation

No.	Project Name	Route	County	Begin milepost	End milepost	Length (mile)
1	003U0007300-NB	US-73	Atchison	0.00	4.14	4.14
2	022K0000700-NB	K-7	Doniphan	5.92	11.71	5.79
3	088U0005400-WB	US-54	Seward	0.00	3.87	3.87
4	091K0002700-NB	K-27	Sherman	0.00	4.19	4.19
5	098U0028300-NB	US-283	Trego	10.03	21.49	11.46
6	103K0003900-NB	K-39	Wilson	14.47	16.43	1.96

Unbound Layer Properties

All projects in this study were full-depth AC pavements except one that has unbound base course layer with crushed stone (AB-3). The resilient modulus of the AB-3 layer was taken as 30,000 psi. A six-inch (150 mm) treated subgrade layer on the original soil was built for all flexible projects. Most of the projects had Lime Treated Subgrade (LTSG) and others are fly-ash-treated subgrade (FATSG), or mechanically stabilized (SUBMOD, untreated). The resilient modulus of lime or fly-ash-treated subgrade was calculated based on Equation 10.

$$LTSGM_R = \left(2.03xUntreated\ M_{R,}\ psi\right) + 225 \qquad (10)$$

Twelve inches of natural soil, under the treated subgrade, was compacted to increase the unit weight and decrease the plasticity of the soil for all projects. KDOT provided information regarding untreated soil resilient modulus for every county, soil gradation, and Atterberg limits which are shown in Table A3 Appendix A.

Traffic Data

The AASHTOWare has three hieratical traffic input levels. level 1 is a project specific traffic information. Level 2 is regional input parameters driven from weigh in motion (WIM) and automatic vehicle classifier (AVC) stations across the state. Level 3 is the software global/default values.

For this study, the available traffic inputs as level 1 data are AADTT, operational speed, number of lanes, and percentage of trucks in the design direction. However, vehicle Class Factor (VCF), Monthly Adjustment Factors (MAFs), Hourly Distribution Factors (HDFs), axle per truck, and axle load spectra were generated as level 2 inputs. These level 2 data inputs were generated from 11 Automated Vehicle Classifier (AVC) and 10 Weigh in Motion (WIM) stations throughout Kansas as shown in Table 3 and 4. The station routes were functionally classified as rural or urban.

Then, the average of the data for the rural route stations was assigned to the rural pavement sections and the same process was repeated for the urban pavement sections.

Climate Data

The geo-coordinates (Latitude and Longitude) for all pavement sections were given as site specific values. Based on KDOT recommendation, the depth of the water table was set at 50 ft. The latest version of AASHTOWare software enables the user to download any climate station file from the FHWA Long Term Pavement Performance (LTPP) site. This feature allows the user to select more accurate climate reports than the previous versions of the software. In this study more accurate climate stations were selected based on the nearest climate station to the project location. Table 5 shows the new exact location for more accurate climate parameters.

Table 3. Kansas WIM stations

WIM Station	County	Route	Functional Classification
2WOA86	Seward	US-54	Rural principal arterial
3MXC22	Meade	US-54	Rural principal arterial
2OPUF5	Logan	US-83	Rural principal arterial
4LGSU3	Thomas	I-70	Rural interstate
9M4PS3	Saline	I-70	Rural interstate
9ORQP1	Sedgwick	I-135	Urban interstate
9Q9OK1	Sedgwick	I-135	Urban interstate
BWGAA6	Lyon	I-35	Urban interstate
DVMSP3	Douglas	I-70	Urban interstate
F07WC7	Wyandotte	I-70	Urban interstate

Table 4. Kansas AVC stations

AVC Station	County	Route	Functional Classification
7XRME7	Kingman	US-54	Rural principal arterial
61ILJ3	Kiowa	US-54	Rural principal arterial
91TFY5	Republic	US-81	Rural principal arterial
AW9N83	Butler	US-400	Rural principal arterial
CTQ1D1	Brown	US-36	Rural principal arterial
CV64B3	Montgomery	I-166	Rural principal arterial
F10VD5	Bourbon	US-61	Rural principal arterial
0DT453	Sherman	I-70	Rural principal arterial
7HOM63	Russel	I-70	Urban principal arterial
9LON61	Sedgwick	I-235	Urban principal arterial
9Q9OK1	Sedgwick	I-135	Urban principal arterial

Calibration Factors of the PMED Performance Models

As mentioned earlier, previous efforts were made for the local calibration of the PMED distress models in Kansas for four types of distress models including, rutting, fatigue cracking, transverse cracking, and IRI. KDOT tracks the overall performance level of the existing flexible pavements by examining/combining the collected distresses. Local calibration of load-related cracking should incorporate alligator and longitudinal cracks as a total fatigue cracking unless cores or trenches were cut from the pavement to confirm the crack the place of crack (AASHTO, 2010). Kansas database does not contain any bottom-up cracking data, hence local calibration was performed for top-down cracking only. Because of the availability of actual measured data for these four types of distresses, only these distress models were locally calibrated.

Table 5. Climate stations selected for the selected projects

Project name	Pavement section location		New selected climate station (version 2.6)	
	latitude (deg)	longitude (deg)	latitude (deg)	longitude (deg)
007U0007500-NB	39.8607	-95.777	39.77	-95.47
008U0005400-EB	37.6994	-96.845	37.86	-96.83
008U0007700-NB-1	37.518	-96.998	37.86	-96.83
008U0007700-NB-2	37.887	-96.849	38	-96.87
008U0007700-NB-3	38.0155	-96.859	38	-96.87
011U0006900-NB	37.1438	-94.832	37.34	-94.8
019K0000700-NB-1	37.4693	-94.627	37.46	-94.62
019K0000700-NB-2	37.3835	-94.833	37.38	-94.83
019U0016000-EB	37.457	-94.836	37.5	-95
023U0004000-EB	38.97	-95.3	37.51	-97.01
025K0009900-NB	37.53	-96.25	37.5	-96.87
027K0015600-EB	38.61	-98.37	38.73	-98.22
028U0005000-EB	37.95	-100.71	38.06	-100.89
031K0001800-WB	39.066	-96.732	38.99	-96.79
033U0028300-NB	39.5184	-99.845	39.31	-99.81
052U0007300-NB	39.401	-95.067	39.31	-94.92
065K0002700-NB	37.134	-101.56	37.13	-101.79
065U0005600-EB	37.05	-101.9	37.13	-101.79
069U0028300-NB	39.914	-99.889	39.83	-99.89
082U0018300-NB	39.176	-99.299	39.5	-99.375
095U0005600-EB	37.17	-101.38	37.5	101.25

The local calibration for the AASHTOWare PMED for Kansas local conditions was done first using version 2.2 (Sufian 2015). Then the local calibration was repeated using version 2.5 (Islam 2019). Table 6 shows the default calibration factors of the AASHTOWare flexible pavement models, and the local calibration factors for Kansas using version 2.2 and 2.5.

For the permanent deformation model, the local calibration efforts relied on changing βR1 and βR2 values in the first trial. Only βR1 was changed in the second trial as shown in Table 6.

Fine subgrade rutting calibration factor βs1 was changed from the default to be 0.4 in the first calibration process, and no further adjustment was needed in the second trial. Not only were the local calibration factors for all distress models changed from the AASHTOWare version 2.2 to version 2.5, but also some default calibration factors as shown in Table 6.

The top-down fatigue cracking calibration factors C1 and C2 changed from the AASHTOWare PMED version 2.2 to version 2.5, globally, and locally. Local calibration factor C1 was changed from 0.9 to 1.9, and C2 was changed from 0.19 to 0.45.

The IRI prediction model coefficients are not globally changed from version to version. However, the IRI C1 and C2 factors have been changed in the first local calibration trial. Then all IRI calibration factors C1, C2, C3, and C4 were adjusted again in the second calibration trial and were determined to be, respectively, 165, 0.1, 0.0031, and 0.002 as shown in Table 3.

Table 6. Global and Local Calibration Factors of Flexible Pavement Design for Versions 2.2 and 2.5

Model	Calibration Coefficient	National/default AASHTOWare version 2.2	Local calibration AASHTOWare version 2.2	National/default AASHTOWare version 2.5	Local calibration AASHTOWare version 2.5
Rutting	βR1	1	0.75	0.4	0.775
	βR2	1	1	0.52	0.52
	βR3	1	0.85	1.36	1.36
	βs1(fine)	1	0.4	1	0.4
	βs1(granular)	1	1	1	1
Top-down fatigue cracking	C1	7	0.9	2.5219	1.9
	C2	3.5	0.45	0.8069	0.19
	C3	-	-	1	1
IRI	C1	40	33	40	165
	C2	0.4	0.4	0.4	0.1
	C3	0.008	0.008	0.008	0.0031
	C4	0.015	0.01	0.015	0.002
Transverse cracking	C1	-	-	0.1	0.1
	C2	-	-	0.9809	0.9809
	C3	-	-	0.19	0.19
	C4	-	-	165.3	133.4
	C5	-	-	-5.1048	-72.4

KDOT Failure Criteria

The accuracy of the transfer function may not be well defined at the values that trigger major rehabilitation (AASHTO 2010). The KDOT-specified threshold distress values for flexible and rigid pavements are listed in Table 7.

Table 7. KDOT specified performance criteria of flexible pavement design

Performance Criteria	KDOT Limit
Terminal IRI (inches/mile)	164
AC top-down fatigue cracking ((% lane area)	25
AC bottom-up fatigue cracking (% lane area)	10
AC thermal cracking (ft/mile)	700
Permanent deformation - total pavement (inches)	0.5
Permanent deformation - AC only (inches)	0.5

These assigned failure criteria specified by KDOT were inserted in the software to evaluate the distresses response with 90% reliability. The evaluation was done using both global/default and local calibration factors. If there is any distress model that did not pass the specified design criteria after applying the local calibration factors, it might indicate the need for recalibration for that distress model. However, it does not mean that there is no need for recalibration of other distress models.

Distresses Results Statistical Analysis

Bias and Standard Error

MEPDG employed global calibration values to compute the performance metrics for individual road sections. These projected values were subsequently assessed against actual measurements to ascertain any bias and Standard Error of Estimation (SEE). This evaluation aimed to validate each distress prediction model, considering local factors such as conditions, policies, specifications, and materials (AASHTO, 2010).

Bias represents the variation between the MEPDG-predicted output values and the observed distresses in the field. If there is a consistent difference between the distress values predicted by the software and those observed in the field, it indicates a statistical bias within the model. Calibration becomes necessary under such circumstances, and this process hinges on the Standard Error of the Estimation (SEE). AASHTO's definition characterizes SEE as the standard deviation of residual errors among the pavement sections integrated into the calibration dataset for each prediction model as mentioned in the literature (AASHTO, 2010). In this study, the bias for both global and local calibration factors will be measured.

Besides addressing bias and the Standard Error of Estimation (SEE), an effort was undertaken to assess the effectiveness of both the global and calibrated performance models through the utilization of the coefficient of determination (R^2). This parameter serves the purpose of quantifying the extent to which the variation in AASHTOWare predicted values, concerning their mean, can be ascribed to a linear association between the predicted data and the actual field measurements (Mendenhall, 2012).

To evaluate the null hypothesis regarding the sampling template, it was necessary to assess bias, and this was accomplished through a paired t-test aimed at initially identifying any bias between the actual distress values and AASHTOWare-predicted data (utilizing globally calibrated coefficients). In standard paired t-test analysis, the objective is to ascertain whether the average difference between two paired sets of samples significantly deviates from zero or a specific target value, as is the case here (Minitab, 2016). The paired t-test in this study quantified the disparities within each dataset containing paired predictions and actual measurements, determined the mean of these disparities, and subsequently assessed whether this mean difference was statistically significant. This examination applied for a paired t-test with a 95% confidence level. The null hypothesis is designed as follows.

$$\text{Hypothesis, } H_0 : \sum(\text{Measured-Predicted}) = 0$$

The decision to accept or reject the null hypothesis relied on the observed significance level, commonly referred to as the p-value. In the context of a 95% confidence level, it was anticipated that the p-value (representing the probability of a particular event occurring) obtained from the paired t-test should be greater than or equal to 0.05 to warrant the acceptance of the null hypothesis. When the null hypothesis was rejected, it signaled the necessity for local bias elimination by calibrating the distress model within the AASHTOWare Pavement ME Design software.

Results

The results part provides the distress models assessment using global and local calibration factors. Additionally, it includes the assessment of local bias and standard error of the estimates from locally and globally calibrated models.

Distress models Assessment

As mentioned earlier, selected pavement projects were analyzed using the AASHTOWare version 2.6.2.2. First the analysis was done using global, or default calibration factors of the software. Then, it was repeated using the local calibration factors developed based on the AASHTOWare version 2.5.0. All flexible projects passed the KDOT failure criteria except top-down fatigue cracking when the local calibration factors developed using AASHTOWare version 2.5 were used. Seven projects failed to satisfy the failure criteria for the top-down fatigue cracking distress model as shown in Table 8. This is because the top-down fatigue cracking model has been changed for the latest version of AASHTOWare. The other distress models have successfully satisfied the failure criteria defined by KDOT. However, this does not mean that the local calibration factor that were previously used are still valid.

Assessment of Bias and Standard Error (SE) of Locally and globally calibrated distress models

Assessment of Globally Calibrated Rutting Model

Local bias was determined by conducting hypothesis testing for the rutting model. Global/default calibration factors were used to predict the rutting distress values. Figure 5 shows these values against the actual measured values. The null hypothesis was rejected at 95% confidence interval. The paired t-test, SE, and correlation coefficient (R^2) are shown in Table 9.

Table 8. Distress response using global and local calibration factors

Project name	IRI (in/mile)		Rutting (in)		Thermal cracking (ft/mile)		Top-down fatigue (% lane area)	
	Global	Local	Global	Local	Global	Local	Global	Local
007U0007500-NB	107.1 (pass)	102.9 (pass)	0.18 (pass)	0.12 (pass)	216.3 (pass)	216.3 (pass)	11.21 (pass)	29.51 (fail)
008U0005400-EB	104.4 (pass)	100.2 (pass)	0.19 (pass)	0.12 (pass)	220 (pass)	220 (pass)	4.69 (pass)	4.69 (pass)
008U0007700-NB-1	107 (pass)	112.1 (pass)	0.24 (pass)	0.19 (pass)	216.4 (pass)	216.4 (pass)	4.69 (pass)	4.69 (pass)
008U0007700-NB-2	105.1 (pass)	101.2 (pass)	0.2 (pass)	0.13 (pass)	216.3 (pass)	216.3 (pass)	4.69 (pass)	4.69 (pass)
008U0007700-NB-3	105.3 (pass)	102.8 (pass)	0.21 (pass)	0.14 (pass)	216.3 (pass)	216.32 (pass)	4.69 (pass)	4.69 (pass)
011U0006900-NB	106.3 (pass)	109.7 (pass)	0.22 (pass)	0.17 (pass)	216 (pass)	216 (pass)	4.69 (pass)	4.69 (pass)
019K0000700-NB-1	104.5 (pass)	102.7 (pass)	0.2 (pass)	0.14 (pass)	216.3 (pass)	216.3 (pass)	4.69 (pass)	4.69 (pass)
019K0000700-NB-2	105.8 (pass)	106.3 (pass)	0.22 (pass)	0.16 (pass)	216.3 (pass)	216.3 (pass)	4.69 (pass)	4.69 (pass)
019U0016000-EB	104.6 (pass)	100.4 (pass)	0.17 (pass)	0.12 (pass)	226.1 (pass)	226.1 (pass)	4.69 (pass)	4.69 (pass)
023U0004000-EB	103.7 (pass)	97.5 (pass)	0.17 (pass)	0.11 (pass)	440.6 (pass)	440.6 (pass)	4.69 (pass)	4.69 (pass)
025K0009900-NB	105.7 (pass)	104.7 (pass)	0.22 (pass)	0.15 (pass)	216.3 (pass)	216.3 (pass)	4.69 (pass)	4.69 (pass)
027K0015600-EB	103.9 (pass)	97.7 (pass)	0.14 (pass)	0.09 (pass)	216 (pass)	216 (pass)	4.69 (pass)	4.69 (fail)
028U0005000-EB	106.1 (pass)	103.2 (pass)	0.18 (pass)	0.13 (pass)	216.3 (pass)	216.3 (pass)	11.57 (pass)	29.65 (fail)
031K0001800-WB	106.2 (pass)	101.5 (pass)	0.18 (pass)	0.12 (pass)	216.3 (pass)	216.3 (pass)	4.69 (pass)	4.69 (fail)
033U0028300-NB	103.3 (pass)	101.1 (pass)	0.17 (pass)	0.13 (pass)	216.3 (pass)	216.3 (pass)	4.69 (pass)	4.69 (pass)
052U0007300-NB	139.3 (pass)	148.4 (pass)	0.3 (pass)	0.2 (pass)	216.3 (pass)	216.3 (pass)	4.69 (pass)	4.69 (pass)
065K0002700-NB	100.5 (pass)	105.0 (pass)	0.17 (pass)	0.15 (pass)	216 (pass)	216 (pass)	4.69 (pass)	4.69 (pass)
065U0005600-EB	99.6 (pass)	98.3 (pass)	0.13 (pass)	0.1 (pass)	216 (pass)	216 (pass)	4.69 (pass)	4.69 (fail)
069U0028300-NB	107.6 (pass)	104.2 (pass)	0.17 (pass)	0.12 (pass)	216 (pass)	216 (pass)	4.69 (pass)	4.69 (pass)
082U0018300-NB	105.2 (pass)	103.3 (pass)	0.17 (pass)	0.13 (pass)	216.3 (pass)	216.3 (pass)	4.69 (pass)	4.69 (fail)
095U0005600-EB	104.0 (pass)	100.3 (pass)	0.15 (pass)	0.11 (pass)	440.6 (pass)	440.6 (pass)	10.21 (pass)	4.69 (fail)

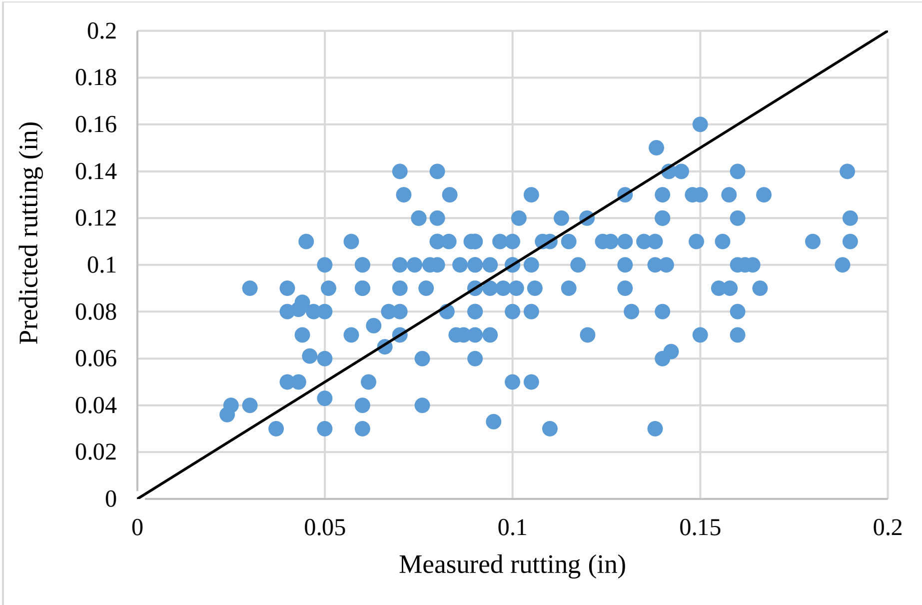

Figure 5. Measured versus predicted rutting response with globally calibrated coefficients

Table 9. Statistical analysis of globally calibrated rutting model

Bias	**SE**	**Se/Sy**	**R^2**	**P-value**	**Hypothesis, $H_{0:}$ ∑(Meas.-Pred.) = 0**
1.62	0.042	0.86	0.52	0.000814	Rejected

As shown in Figure 5, it is obvious that the predicted rutting values versus the measured values are spread around the line. It does not show a good linearity, however, the bias looks acceptable despite the rejection of null hypotheses. Additionally, it seems that the default calibration factor for the latest version might not need extensive change in the calibration factors to be locally calibrated. It seems that it needs adjustment to the bias.

Elimination of Local Bias of the Rutting Model

From Equations 1 it can be observed that the calibration parameters β_{1r}, can be optimized outside of the AASHTOWare. Since the model shows a slight bias and acceptable standard error,

β_{1r} was adjusted to reduce bias. Generalized Reduced Gradient (GRG) nonlinear optimization technique was performed using Microsoft Excel Solver to optimize β_{1r}.

The adjusted coefficient was used as the locally calibrated coefficient in the permanent deformation model of the AASHTOWare Pavement ME Design software, and a paired t-test was conducted between the measured and new predicted data. The values of the calibrated new values versus the measured values are shown in Figure 6. The results of the paired t-test after the calibration are shown in Table 10. The null hypothesis was accepted for the calibrated model. It seems that the bias reduced from 1.62 to 0.3.

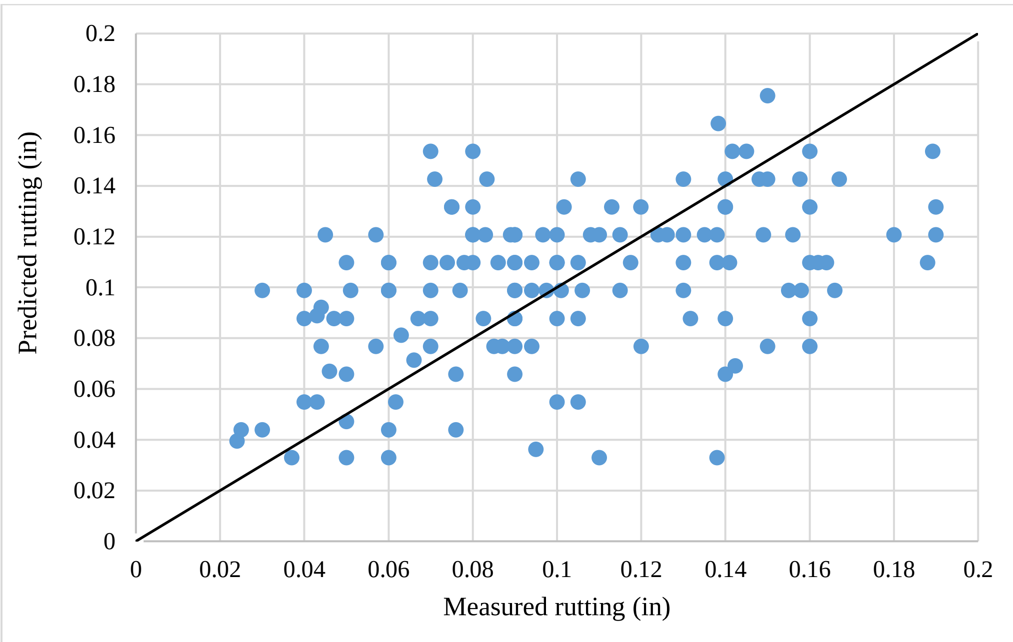

Figure 6. Measured versus predicted rutting response with locally calibrated coefficients

Table 10. Statistical analysis of locally calibrated rutting model

Bias	SE	Se/Sy	R^2	P-value	Hypothesis, H_0: ∑(Meas.-Pred.) = 0
0.3	0.04	0.86	0.52	1.66	Accepted

Results in Table 10 show that the standard error of estimate (SE) has decreased slightly after local calibration (0.04 in). The local calibration guide for the AASHTOWare software recommends that the standard error of estimate of the permanent deformation model be within 0.10 in, which means that the criteria has been met.

The statistical analysis results for testing the five validation projects are shown in Table 11. The null hypothesis was accepted with a standard error below the recommended value. After completion of local calibration, the coefficients shown in Table 12 were selected for the permanent deformation model. The adjusted coefficients are shown in bold.

Table 11. Statistical analysis of locally calibrated rutting model for validation projects

Bias	SE	Se/Sy	R^2	P-value	Hypothesis, H_0: ∑(Meas.-Pred.) = 0
-0.13	0.04	1.08	0.4	0.35	Accepted

Table 12. Local calibration factors of rutting model

Br_1	Br_2	Br_3
0.176	0.52	1.36

Assessment of Globally Calibrated IRI Model

Local bias was determined by conducting hypothesis testing for the IRI model. Global/default calibration factors were used to predict the rutting distress values. Figure 7 shows these values against the actual measured values. The null hypothesis was rejected at 95% confidence interval. The paired t-test, SE, and correlation coefficient (R^2) are shown in Table 13. The bias of the results is -385, and the SE is 10. The correlation between predicted and measured is found to be 0.46, which is considered relatively weak.

As shown in Figure 7, it is obvious that the predicted IRI values versus the measured values are not widespread along the equality line. It does not show a good fit because most predicted IRI distress values are very close for all have close values of IRI model.

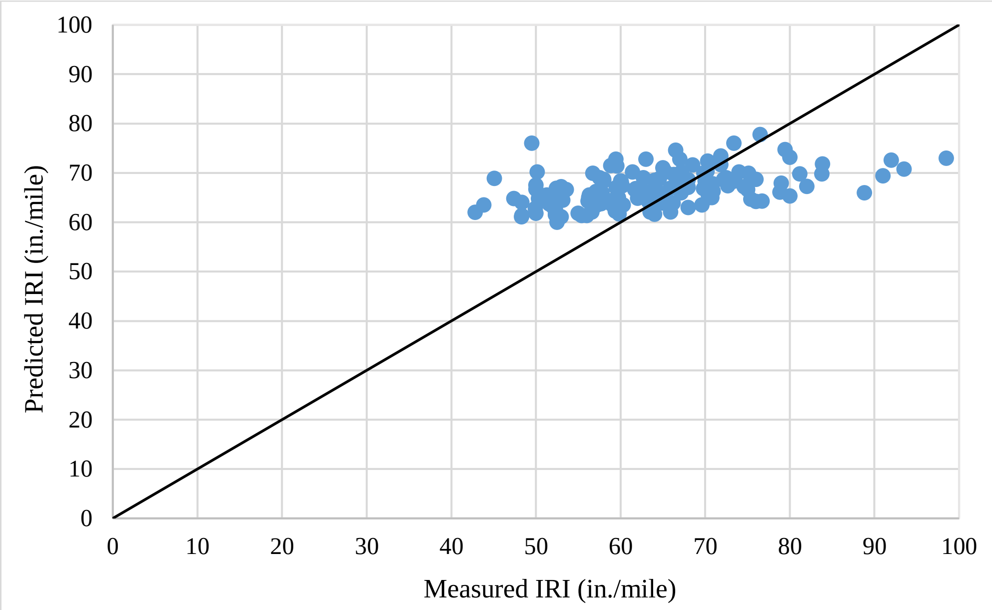

Figure 7. Measured versus predicted IRI response with globally calibrated coefficients

Table 13. Statistical analysis of globally calibrated IRI model

Bias	SE	Se/Sy	R^2	P-value	Hypothesis, H_0 : $\sum$(Meas.-Pred.) = 0
-385	10	0.9	0.46	0.003	Rejected

Elimination of Local Bias of IRI Model

From Equation 3, it can be observed that the data for subgrade soil percent passing the 0.02 and 0.075 sieve are required to calculate the site factor parameter. These data were extracted from the soil properties given by the KDOT and then the site factor was calculated and used for the optimization process. As shown in Equation 3, C2 and C3 calibration factors are directly multiplied by the fatigue and transverse cracking, respectively. Since most of the output of the fatigue and transverse cracking values are zeros, it is infeasible to modify these two factors. C1 and C4 were optimized outside the AASHTOWare using the solver techniques within Microsoft Excel. The calibrated values are plotted versus the measured value as shown in Figure 8. Table 14 shows that the bias has significantly reduced to -161 with a slight better correlation between the actual and predicted IRI values.

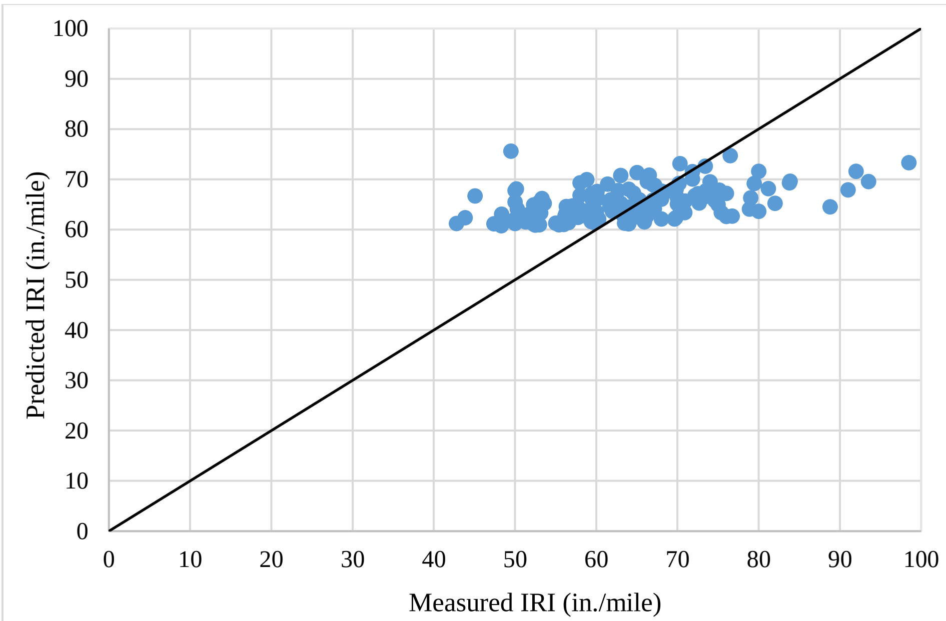

Figure 8. Measured versus predicted IRI response with locally calibrated coefficients

Table 14. Statistical analysis of locally calibrated IRI model

Bias	SE	Se/Sy	R^2	P-value	Hypothesis, H_0: ∑(Meas.-Pred.) = 0
-161	10.1	0.9	0.45	0.09	Accepted

The statistical analysis results of testing IRI model for the five validation projects are shown in Table 15. The null hypothesis was accepted with a lower bias of -33.15. However, it can be seen from the results that the standard error of estimate has increased slightly from 10.1 to 12.8 after calibration. The four components of standard error were previously discussed in this report, and it was mentioned that that the distress/IRI measurement error is a major contributor among the error components. Nonetheless, the design guide recommends that the standard error of the estimates of the IRI model should be within 17 in/mile which was satisfied.

After completion of local calibration, the coefficients shown in Table 16 were selected for the permanent deformation model. The adjusted coefficients are shown in bold.

Table 15. Statistical analysis of locally calibrated IRI model for validation projects

Bias	Se	Se/Sy	R^2	P-value	Hypothesis, H_0: $\sum$(Meas.-Pred.) = 0
-33.15	12.8	0.8	0.7	0.34	Accepted

Table 16. Local calibration factors of IRI model

C1	C2	C3	C4
17.75	0.4	0.008	**0.0307**

Assessment of Globally Calibrated Top-Down Fatigue Cracking Model

Local bias was determined by conducting hypothesis testing for the top-down fatigue cracking model. Global/default calibration factors were used to predict the fatigue cracking distress values. This new distress function for the top-down fatigue cracking model has been developed lately. Figure shows these values against the actual measured values. All the top-down fatigue crack output values are zeros except for two projects (007U0007500-NB, 28U0005000-EB) when measured at 50% reliability as shown in figure. The model showed significant bias in the paired t-test and the null hypothesis was rejected at 95% confidence interval as shown in Table 17.

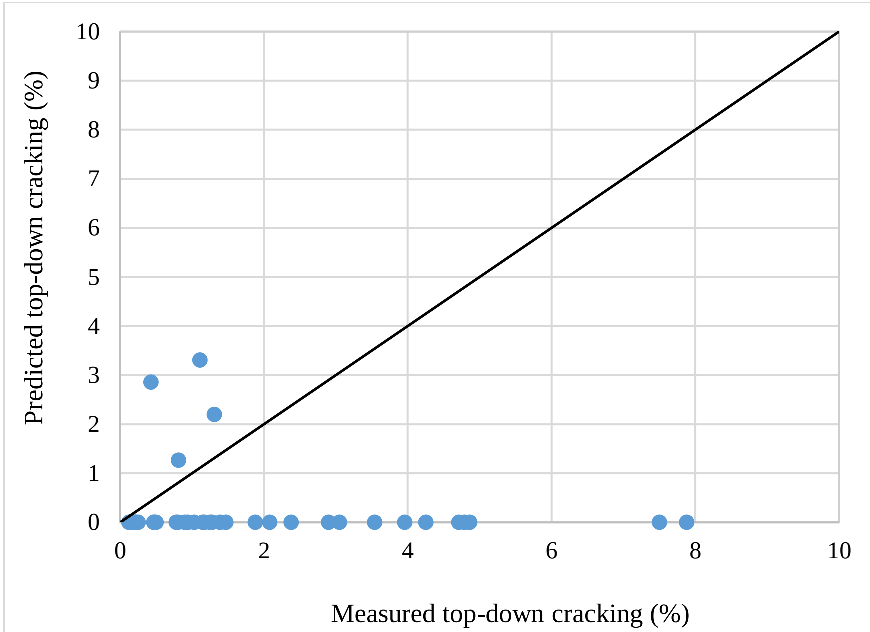

Figure 9. Measured versus predicted top-down fatigue model response with globally calibrated coefficients

Table 17. Statistical analysis of locally calibrated top-down fatigue model

Bias	SE	R^2	p-value	Hypothesis, H_0 : ∑(Meas.-Pred.) = 0
214	6	0.18	< 0.0001	Rejected

Elimination of Local Bias of Top-Down Fatigue Cracking Model

Since it is hard to optimize the data outside the program due to all the inputs in Equations 5 and 6 sensitivity analysis that has been done for all the top-down calibration factors. All projects gave zero values for the top-down cracking along the design period with multiple different trial to adjust the calibration factors except the two projects mentioned earlier. The analysis for 50% reliability produces zero percent fatigue cracking along the design period for all projects with any changes in calibration factors as shown in Figure 10. The analysis for 90% reliability produces constant value 4.69 percent fatigue cracking along the design period for all projects as shown with any changes in calibration factors as shown in Figure 11. Figures 12 and 13 show the fatigue response of project 007U0007500-NB at 50% and 90% reliability, respectively. The same trend of fatigue cracking for project 007U0007500-NB has been observed for project 28U0005000-EB unlike all other projects.

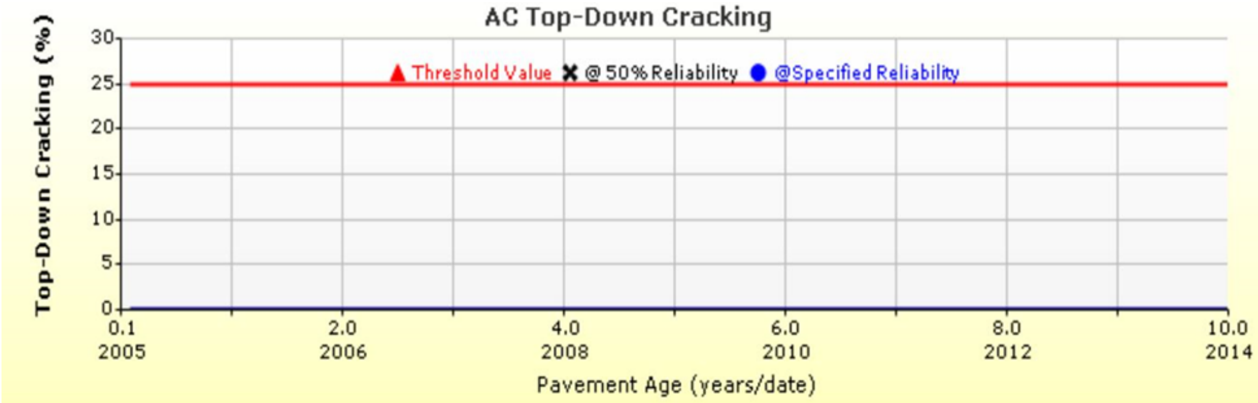

Figure 10. Top-down fatigue cracking response versus time for most projects at 50% Reliability

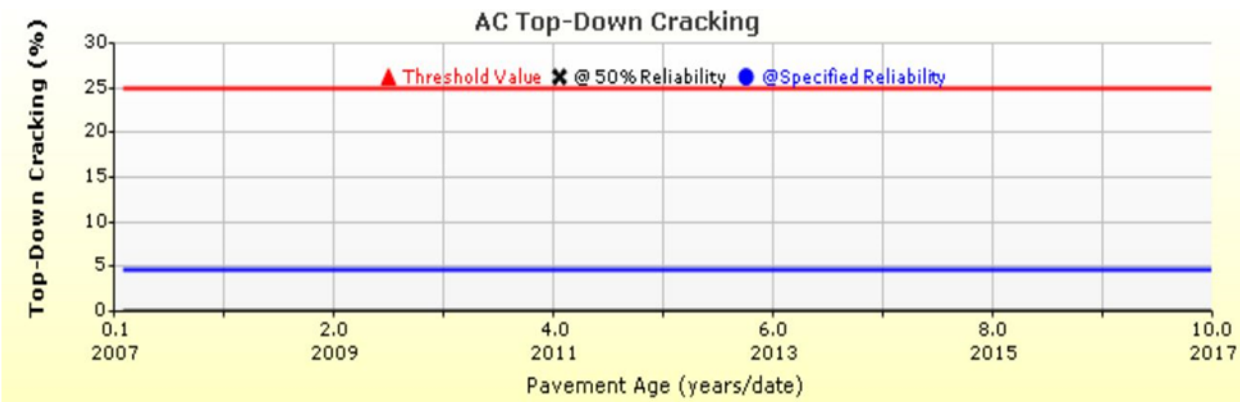

Figure 11. Top-down fatigue cracking response versus time for all projects at 90% Reliability

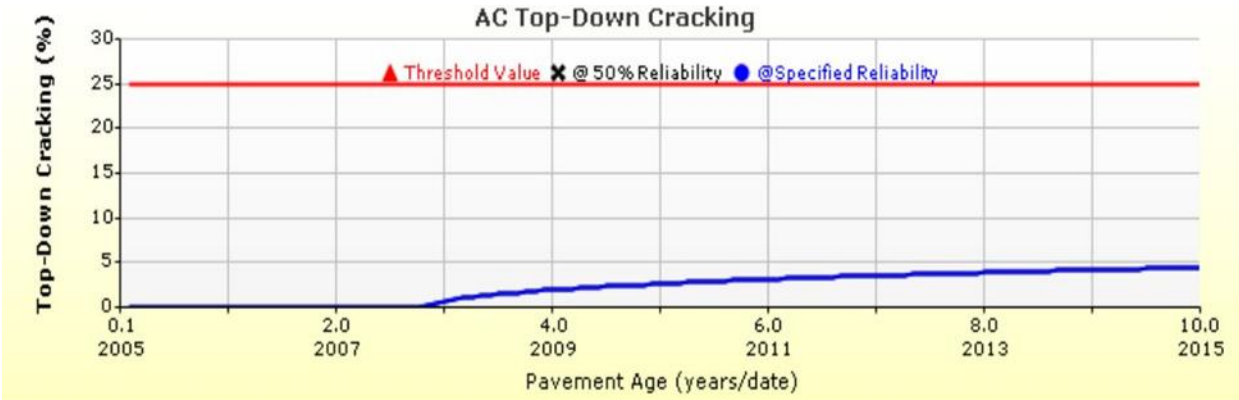

Figure 12. Top-Down fatigue cracking response for project 007U0007500-NB at 50% Reliability

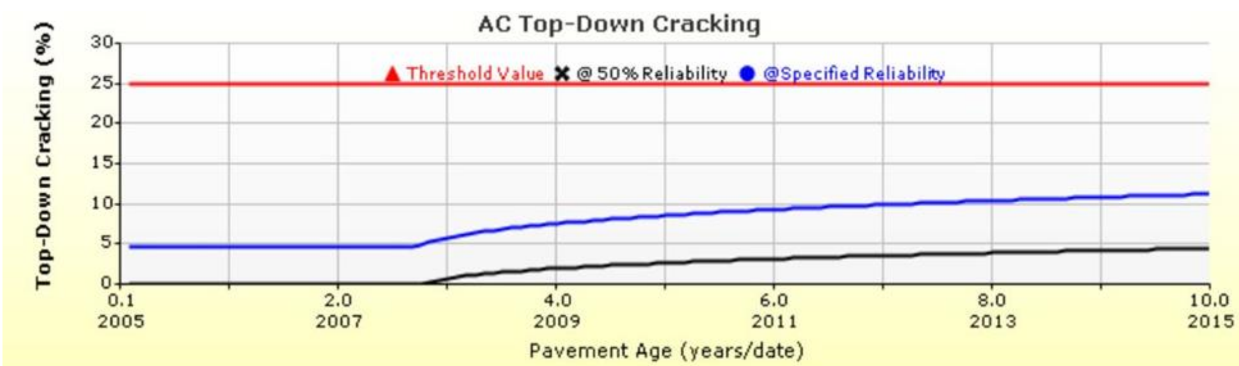

Figure 13. Top-Down fatigue cracking response for project 007U0007500-NB at 90% Reliability

After considering the results and figures of fatigue cracking, it was observed that the AASHTOWare produced normal top-down fatigue cracking results for only two projects (007U0007500-NB, 28U0005000-EB). It was observed that these two projects are the only projects that have the highest AADTT (1000, 1170). This is typically inconsistent with the findings of NCHRP report which states that time to crack initiation (t_0) is calculated from regression equation as a function of AADTT (NCHRP 2018). The reason that the AASHTOWare produced zero top-down fatigue values for all the projects with any changes in calibration factors may be because the AADTT for all projects are relatively low (below 1000). Hence, it is not possible to adjust the calibration factors for the top-down fatigue cracking based on these projects. For implementing a local calibration of the new top-down fatigue cracking model, a new group of flexible pavements should be selected with high AADTT number (higher than 1000).

Assessment of Globally Calibrated Thermal Cracking Model

The bias was determined by conducting hypothesis testing for the AC thermal cracking model with the globally calibrated coefficients. The measured versus predicted thermal cracking is shown in Figure 14. Paired t-test at 95% confidence level resulted in p-value lower than 0.05 indicating presence of significant bias in the thermal fracture model. The statistical analysis results are shown in Table 18. Figure 14 shows a significant difference between the measured and predicted transverse cracking. The standard error of estimate was found to be 99 ft/mile. AASHTO recommends that the standard error of estimate be within 250 ft/mile.

Elimination of Local Bias of Thermal Cracking Model

Only 13 projects out of 27 projects showed transverse cracking response. Also, Level 1 input (creep compliance and indirect tensile strength) data for this study was not available. Additionally, most of KDOT measured data of transverse cracking are zeros. Thus, it was decided that the AC thermal cracking model should be calibrated by district for KDOT and only the districts showing AC transverse cracking should be calibrated in the future. Further attempts to calibrate the model was not carried out in this phase of the study.

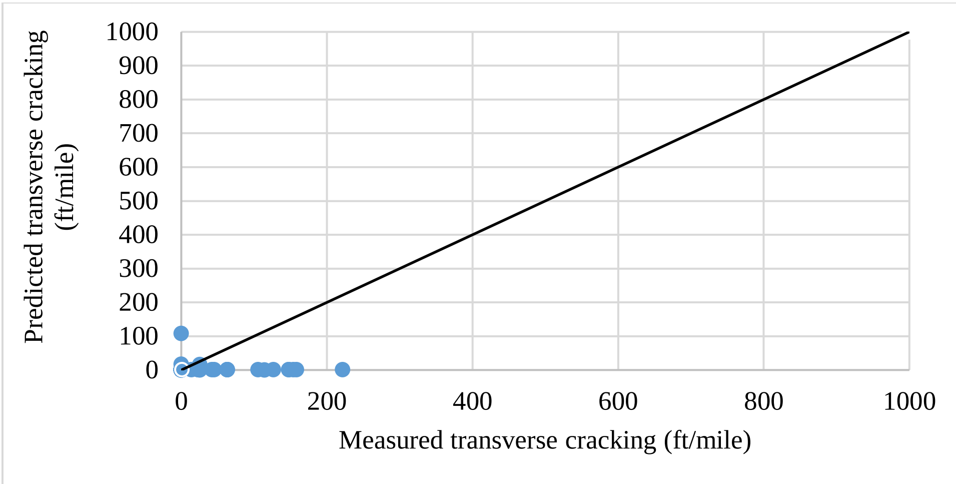

Figure 14. Measured versus predicted transverse cracking model response with globally calibrated coefficients

Table 18. Statistical analysis of locally calibrated transverse cracking model

Bias	SE	R^2	p-value	Hypothesis, H_0 : ∑(Meas.-Pred.) = 0
2425	99	0.015	< 0.0001	Rejected

Discussion

The twenty-one-flexible pavement project analysis using the AASHTOWare version 2.6.2. showed that seven projects failed to satisfy the failure criteria for the top-down fatigue cracking distress model. This is because the top-down fatigue cracking model has been changed for the latest version of AASHTOWare. The other distress models have been successfully satisfied the failure criteria by KDOT. However, this does not mean that the local calibration factors that were previously produced are still valid to be used for the local design. For every distress model, there is a reason for rejecting the validity of the previously produced local calibration factors.

Rutting model

The results of the statistical analysis of rutting model using local calibration factors version 2.5.0 showed less SE of the estimates and R^2 than the rutting model using globally calibration factors version 2.6.2.2 as shown in Table 19. However, the null hypothesis was rejected because the locally calibrated model showed a higher bias. After adjusting the bias using only one calibration factor, it results in a better model. This may indicate that the local calibration factors for the new version 2.6.2.2 have a better ability to predict the rutting distress for Kansas region without calibration process.

Table 19. Comparison between local and global calibration models of the newest version and 2.5.0 version for rutting model

Calibration type	Bias	SE	R^2	p-value	Hypothesis, H_0 : $\sum$(Meas.-Pred.) = 0
Local 2.5.0	-0.81	0.05	0.37	0.134	Accepted
Global 2.6.2	1.82	0.042	0.52	0.0008	Rejected
Local 2.6.0	0.3	0.04	0.52	1.66	Accepted

IRI Model

The results of the statistical analysis of IRI model using local calibration factors version 2.5.0 showed less SE of the estimates and R^2, and higher bias than the rutting model using locally calibration factors version 2.6.2 as shown in Table 20. This may indicate that a better calibration factors of the IRI model could be used for better prediction.

Table 20. Comparison between local calibration models of the newest version and 2.5.0 version for IRI model

Calibration type	Bias	SE	R^2	p-value	Hypothesis, H_0 : $\sum$(Meas.-Pred.) = 0
Local 2.5.0	-215.8	10.13	0.22	0.077	Accepted
Local2.6.2	-161	10.0	0.45	0.09	Accepted

Top-Down Fatigue Cracking Model

As mentioned Earlier the distress function of top-down fatigue cracking model has been changed at the latest version. However, it was not possible to implement the calibration process because all the given projects have AADT less than 1000 (Saleh et al., 2023). The top-down distress model does not give any changeable response with changing the calibration factors for the projects that have AADT less than 1000. Thus, any future trials to calculate the local calibration factor for this model other projects should be used.

Transverse Fatigue Cracking Model

The actual measured data for transverse cracking are not enough to start a calibration process. In addition, the basic inputs that are responsible for the thermal fatigue prediction (creep compliance and indirect tensile strength) were used as default values. Hence, the current available projects are not convenient for the local calibration process of the transverse cracking the top-down fatigue cracking models.

Conclusions and Recommendations

Since the latest version of AASHTOWare 2.6.2.2 PMED has been released, the calibration factors of performance models need to be tested globally, and locally. The main objective of this study is to find the distresses response of pavements in-service using the global, and local calibration factors for Kansas region. Then, evaluating the results based on bias, residuals, and standard error between the measured and predicted distresses. The final findings and recommendations were found to be as follow:

- Rutting, IRI, transverse cracking models have successfully satisfied the failure criteria set by KDOT. However, this does not imply that the local calibration factors that were previously determined for Kansas are still valid.
- Global calibration factor of version 2.6.2.2 for rutting distress shows a better SE value and correlation than using the previously evaluated local calibration factors using version 2.5.0.
- AASHTO has introduced a new model for top-down fatigue cracking prediction in MEPDG which mainly rely on the AADTT parameter.
- Flexible pavements projects with AADTT higher than 1000 are needed for the local calibration of the new top-down fatigue cracking model.
- The transverse cracking model needs more actual measurements from the KDOT, so the local calibration process could be implemented.
- More specific material properties (level 1) are needed for every project including Indirect tensile Strength, creep compliance, and asphalt dynamic modulus for better and accurate stresses prediction and calibration.

References

AASHTO. (1993). "AASHTO Guide for Design of Pavement Structures," American Association of State Highway and Transportation Officials, Vol. 1, AASHTO.

AASHTO. (2010). "Guide for the Local Calibration of the Mechanistic-Empirical Pavement Design Guide," American Association of State Highway and Transportation Officials, Washington, D.C.

AASHTO. (2014). "AASHTOWare Pavement ME Design Software Help System," American Association of State Highway and Transportation Officials, Washington, D.C.

AASHTO. (2015). "Mechanistic-Empirical Pavement Design Guide: A Manual of Practice," American Association of State Highway and Transportation Officials, Washington, D.C.

AASHTO. (2008). "Mechanistic-empirical pavement design guide: A manual of practice," Interim edition, American Association of State Highway and Transportation Officials, Washington, DC.

FHWA. (2011). "Implementing Mechanistic-Empirical Pavement Design and Darwin-ME," Federal Highway Administration, Office of Pavement Technology.

FHWA. (2014). "Table HM-12 in Highway Statistics 2014," Office of Highway Policy Information, U.S. Department of Transportation, Federal Highway Administration, Washington, D.C., http://www.fhwa.dot.gov/policyinformation/statistics/2008/hm12.cfm.

Huang, Y. H. (1993). "Pavement analysis and design", Vol. 2, pp. 401-409. Upper Saddle River, NJ: Pearson Prentice Hall, 2004.

Khanum, T. (2005). "Kansas Rigid Pavement Analysis Following New Mechanistic-Empirical Design Guide," master's thesis, Kansas State University, Manhattan, Kansas.

Kim, Y. R., Jadoun, F. M., Hou, T., and Muthadi, N. (2011). "Local calibration of the MEPDG for flexible pavement design," No. FHWA\ NC\ 2007-07, NC Department of Transportation Research and Analysis Group, North Carolina Department of Transportation, Raleigh, North Carolina.

Kou, C., Xiao, P., Kang, A., Mikhailenko, P., Baaj, H., & Wu, Z. (2017). "Methods to evaluate the aging grades of reclaimed asphalt binder". Applied Sciences No, 7(12), 1209.

Ksaibati, K., and Kasperick, T (2013). "Calibration of the mechanistic-empirical pavement design guide for local paved roads in Wyoming". No. MPC\15-294. Mountain Plains Consortium.

Islam, S., Sufian, A., Tavakol, M., & Hossain, M. (2016). "Effect of RAP and RAS Mixture on Flexible Pavement Design". No. 16-5775.

Islam, S. (2019). “Implementation of AASHTOWare Pavement ME Design Software for Pavement Rehabilitation”. Kansas State University.

Mendenhall, W. and Sincich, T. (2012). A Second Course in Statistics Regression Analysis. Prentice Hall.

Minitab Support. (2016). “Hypothesis Tests,” <http://support.minitab.com/en-us/minitab/17/topic-library/basic-statistics-and graphs/hypothesis-tests/tests-of-means/why-use-paired-t/> (accessed on September 21, 2016).

Nantung, T., Chehab, G., Newbolds, S., Galal, K., Li, S., & Kim, D. H. (2005). “Implementation Initiatives of the Mechanistic–Empirical Pavement Design Guides in Indian Transportation Research Record”, 1919(1), 142-151.Construction Field Service Division.

National Cooperative Highway Research Program, (2014). “AASHTO Guide for Design of Pavement Structures”. NCHRP Report 673.

NCHRP (National Academies of Sciences, Engineering, and Medicine). (2018). "A Mechanistic–Empirical Model for Top–Down Cracking of Asphalt Pavements Layers."

NHI. (2002). “Introduction to Mechanistic-Empirical Pavement Design of New and Rehabilitated Pavements,” Course No. 131064, National Highway Institute, Federal Highway Administration, Washington, D.C.

Saleh, N. S., Hossain, M., & Velasquez Jr, N. (2023) “Local Calibration of AASHTOWare Flexible Pavement Mechanistic Empirical Design Software for Kansas”. In Airfield and Highway Pavements 2023 (pp. 34-44).

Qiang, et al. (2011). “Mechanistic-empirical pavement design guide (MEPDG)”. a bird’s-eye view. Journal of Modern Transportation, No. 19.2 114-133.

Robbins, et al. (2017). “Pavement ME design–A summary of local calibration efforts for flexible pavements” NCAT Rep: 1-98.

Timm, D., Birgisson, B., and Newcomb, D. (1998). “Development of mechanistic-empirical pavement design in Minnesota,” In Transportation Research Record: Journal of the Transportation Research Board. No.1629, Transportation Research Board of the National Academies, Washington, D.C., pp. 181-188.

Sufian, A. A. (2016). “Local calibration of the mechanistic empirical pavement design guide for Kansas” master’s thesis, Kansas State University, Manhattan, Kansas. (Master, Kansas State University).

Appendix A - structural information of the flexible pavements

Table A 1. Summary of the structural information of flexible pavements

Project Name	Layer No.	Layer type	Material Type	Thickness (in)
003U0007300-NB	1	Flexible	SM 9.5T	1.5
	2	Flexible	SM 19A	2.5
	3	Flexible	SM 19A	6.5
	4	Subgrade	LIMESUB	6.0
	5	Subgrade	A-7-6 (compacted)	12
	6	Subgrade	A-7-6	Semi-infinite
007U0007500-NB	1	Flexible	SM 9.5A	1.5
	2	Flexible	SM 19A	2.5
	3	Flexible	SM 19A	11.8
	4	Subgrade	LIMESUB	6.0
	5	Subgrade	A-7-6 (compacted)	12
	6	Subgrade	A-7-6	Semi-infinite
008U0007700-NB-1	1	Flexible	SM 9.5T	1.5
	2	Flexible	SM 19A	2.5
	3	Flexible	SM 19A	6.5
	4	Subgrade	LIMESUB	6.0
	5	Subgrade	A-7-6 (compacted)	12
	6	Subgrade	A-7-6	Semi-infinite
008U0007700-NB-2	1	Flexible	SM 9.5A	1.5
	2	Flexible	SM 19A	2.5
	3	Flexible	SM 19A	8.7
	4	Subgrade	LIMESUB	6.0
	5	Subgrade	A-7-6 (compacted)	12
	6	Subgrade	A-7-6	Semi-infinite
008U0007700-NB-3	1	Flexible	SM 9.5A	1.5
	2	Flexible	SM 19A	2.5
	3	Flexible	SM 19A	6.5
	4	Subgrade	LIMESUB	6.0
	5	Subgrade	A-7-6 (compacted)	12
	6	Subgrade	A-7-6	Semi-infinite

Project Name	Layer No.	Layer type	Material Type	Thickness (in)
008U0005400-EB	1	Flexible	SM 9.5T	1.5
	2	Flexible	SM 19A	2.5
	3	Flexible	SM 19A	8.7
	4	Subgrade	LIMESUB	6.0
	5	Subgrade	A-7-6 (compacted)	12
	6	Subgrade	A-7-6	Semi-infinite
011U0006900-NB	1	Flexible	SM 9.5T	1.5
	2	Flexible	SM 19A	2.5
	3	Flexible	SM 19A	6.3
	4	Subgrade	LIMESUB	6.0
	5	Subgrade	A-7-6 (compacted)	12
	6	Subgrade	A-7-6	Semi-infinite
019K0000700-NB-1	1	Flexible	SM 9.5A	1.5
	2	Flexible	SM 19A	2.5
	3	Flexible	SM 19A	7.9
	4	Subgrade	LIMESUB	6.0
	5	Subgrade	A-7-6 (compacted)	12
	6	Subgrade	A-7-6	Semi-infinite
019K0000700-NB-2	1	Flexible	SM 9.5A	1.5
	2	Flexible	SM 19A	2.5
	3	Flexible	SM 19A	6.3
	4	Subgrade	LIMESUB	6.0
	5	Subgrade	A-7-6 (compacted)	12
	6	Subgrade	A-7-6	Semi-infinite
019U0016000-EB	1	Flexible	SM 9.5T	1.4
	2	Flexible	SM 19A	2.5
	3	Flexible	SM 19A	7.1
	4	Non-Stabilized Base	AB-3	6.0
	5	Subgrade	A-7-6 (compacted)	12
	6	Subgrade	A-7-6	Semi-infinite

Project Name	Layer No.	Layer type	Material Type	Thickness (in)
022K0000700-NB	1	Flexible	SM 9.5T	1.5
	2	Flexible	SM 19A	2.5
	3	Flexible	SM 19A	4.7
	4	Non-Stabilized Base	AB-3	11
	5	Subgrade	FLYSUB	6.0
	6	Subgrade	A-7-6 (compacted)	Semi-infinite
023U0004000-EB	1	Flexible	SM 9.5A	1.5
	2	Flexible	SM 19A	2.5
	3	Flexible	SM 19A	8.7
	4	Subgrade	LIMESUB	6.0
	5	Subgrade	A-7-6 (compacted)	12
	6	Subgrade	A-7-6	Semi-infinite
025K0009900-NB	1	Flexible	SM 9.5A	1.5
	2	Flexible	SM 19A	2.5
	3	Flexible	SM 19A	7.1
	4	Subgrade	LIMESUB	6.0
	5	Subgrade	A-7-6 (compacted)	12
	6	Subgrade	A-7-6	Semi-infinite
027K0015600-EB	1	Flexible	SM 9.5A	1.5
	2	Flexible	SM 19A	2.5
	3	Flexible	SM 19A	11
	4	Subgrade	LIMESUB	6.0
	5	Subgrade	A-7-6 (compacted)	12
	6	Subgrade	A-7-6	Semi-infinite
028U0005000-EB	1	Flexible	SM 9.5T	1.5
	2	Flexible	SM 19A	2.5
	3	Flexible	SM 19A	11
	4	Subgrade	LIMESUB	6.0
	5	Subgrade	A-7-6 (compacted)	12
	6	Subgrade	A-7-6	Semi-infinite

Project Name	Layer No.	Layer type	Material Type	Thickness (in)
031K0001800-WB	1	Flexible	SM 9.5T	1.5
	2	Flexible	SM 19A	2.5
	3	Flexible	SM 19A	10.2
	4	Subgrade	LIMESUB	6.0
	5	Subgrade	A-7-6 (compacted)	12
	6	Subgrade	A-7-6	Semi-infinite
033U0028300-NB	1	Flexible	SM 9.5A	1.5
	2	Flexible	SM 19A	2.5
	3	Flexible	SM 19A	9.4
	4	Subgrade	SUBMOD	6.5
	5	Subgrade	A-7-6 (compacted)	12
	6	Subgrade	A-7-6	Semi-infinite
052U0007300-NB	1	Flexible	SM 9.5T	1.5
	2	Flexible	SM 19A	2.5
	3	Flexible	SM 19A	6.5
	4	Subgrade	LIMESUB	6.0
	5	Subgrade	A-7-6 (compacted)	12
	6	Subgrade	A-7-6	Semi-infinite
065K0002700-NB	1	Flexible	SM 9.5T	1.5
	2	Flexible	SM 19A	2.5
	3	Flexible	SM 19A	7
	4	Subgrade	SUBMOD	6.0
	5	Subgrade	A-7-6 (compacted)	12
	6	Subgrade	A-7-6	Semi-infinite
065U0005600-EB	1	Flexible	SM 9.5T	1.5
	2	Flexible	SM 19B	2.5
	3	Flexible	SM 19A	9.4
	4	Subgrade	SUBMOD	6.0
	5	Subgrade	A-7-6 (compacted)	12
	6	Subgrade	A-7-6	Semi-infinite

Project Name	Layer No.	Layer type	Material Type	Thickness (in)
069U0028300-NB	1	Flexible	SM 9.5T	1.5
	2	Flexible	SM 19B	2.5
	3	Flexible	SM 19A	9.4
	4	Subgrade	SUBMOD	6.0
	5	Subgrade	A-7-6 (compacted)	12
	6	Subgrade	A-7-6	Semi-infinite
082U0018300-NB	1	Flexible	SM 9.5T	1.5
	2	Flexible	SM 19A	2.5
	3	Flexible	SM 19A	9.4
	4	Subgrade	FLYSUB	6.0
	5	Subgrade	A-7-6 (compacted)	12
	6	Subgrade	A-7-6	Semi-infinite
088U0005400-WB	1	Flexible	SM 9.5T	1.5
	2	Flexible	SM 19A	2.5
	3	Flexible	SM 19A	13.4
	4	Subgrade	FLYSUB	6.0
	5	Subgrade	A-7-6 (compacted)	12
	6	Subgrade	A-7-6	Semi-infinite
091K0002700-NB	1	Flexible	SM 9.5T	1.5
	2	Flexible	SM 19B	2.5
	3	Flexible	SM 19A	8.7
	4	Subgrade	SUBMOD	6.0
	5	Subgrade	A-7-6 (compacted)	12
	6	Subgrade	A-7-6	Semi-infinite

Project Name	Layer No.	Layer type	Material Type	Thickness (in)
095U0005600-EB	1	Flexible	SM 9.5T	1.5
	2	Flexible	SM 19A	2.5
	3	Flexible	SM 19A	9.4
	4	Subgrade	FLYSUB	6.0
	5	Subgrade	A-7-6 (compacted)	12
	6	Subgrade	A-7-6	Semi-infinite
098U0028300-NB	1	Flexible	SM 9.5T	1.5
	2	Flexible	SM 19A	2.5
	3	Flexible	SM 19A	8.7
	4	Subgrade	LIMESUB	6.0
	5	Subgrade	A-7-6 (compacted)	12
	6	Subgrade	A-7-6	Semi-infinite
103K0003900-NB	1	Flexible	SM 9.5T	1.5
	2	Flexible	SM 19A	2.5
	3	Flexible	SM 19A	5.5
	4	Subgrade	SUBMOD	6.0
	5	Subgrade	A-7-6 (compacted)	12
	6	Subgrade	A-7-6	Semi-infinite

Table A 2. Site-specific material properties for new flexible pavements

Project Name	Pavement Layer	Binder Grade	Binder Content (By Volume)	Gradation (% Passing)			
				3/4″	3/8″	#4	#200
007U0007500-NB	Surface Course	PG 70-28	11.6	100	98	78	3
	Binder Course	PG 64-22	11	95	82	69	3
	Base Course	PG 70-22	10.1	95	82	69	3
Project Name	Pavement Layer	Binder Grade	Binder Content	Gradation			
				3/4″	3/8″	#4	#200
008U0007700-NB-1	Surface Course	PG 64-28	12.2	100	98	70	5
	Binder Course	PG 64-28	9.9	98	84	66	5
	Base Course	PG 64-28	9.9	98	84	66	5
Project Name	Pavement Layer	Binder Grade	Binder Content	Gradation			
				3/4″	3/8″	#4	#200
008U0007700-NB-2	Surface Course	PG 64-28	12.4	100	98	79	4
	Binder Course	PG 64-28	9.9	98	78	60	5
	Base Course	PG 64-28	9.7	99	79	40	3
Project Name	Pavement Layer	Binder Grade	Binder Content	Gradation			
				3/4″	3/8″	#4	#200
008U0007700-NB-3	Surface Course	PG 64-28	11.6	100	97	77	4
	Binder Course	PG 64-28	10.2	97	83	64	5
	Base Course	PG 64-22	9.2	98	83	63	3
Project Name	Pavement Layer	Binder Grade	Binder Content	Gradation			
				3/4″	3/8″	#4	#200
008U0005400-EB	Surface Course	PG 64-28	12.3	100	98	73	5
	Binder Course	PG 64-28	10.7	97	82	63	4
	Base Course	PG 64-22	10.1	97	83	66	4

Project Name	Pavement Layer	Binder Grade	Binder Content	Gradation			
				3/4″	3/8″	#4	#200
011U0006900-NB	Surface Course	PG 64-28	12	100	98	70	5
	Binder Course	PG 64-28	10.9	95	82	57	4
	Base Course	PG 64-22	11.1	97	82	59	3
Project Name	Pavement Layer	Binder Grade	Binder Content	Gradation			
				3/4″	3/8″	#4	#200
019K0000700-NB-1	Surface Course	PG 64-28	10.3	100	96	74	4
	Binder Course	PG 64-28	10.9	100	76	53	3
	Base Course	PG64-22	10.9	100	79	50	2
Project Name	Pavement Layer	Binder Grade	Binder Content	Gradation			
				3/4″	3/8″	#4	#200
019K0000700-NB-2	Surface Course	PG 64-28	12.4	100	94	71	3
	Binder Course	PG 64-28	11.1	99	82	60	2
	Base Course	PG 64-22	10.5	100	78	60	3
Project Name	Pavement Layer	Binder Grade	Binder Content	Gradation			
				3/4″	3/8″	#4	#200
019U0016000-EB	Surface Course	PG 64-22	10	100	98	63	4
	Binder Course	PG 64-22	9.2	98	83	63	3
	Base Course	PG 64-22	9.2	98	83	63	3
Project Name	Pavement Layer	Binder Grade	Binder Content	Gradation			
				3/4″	3/8″	#4	#200
023U0004000-EB	Surface Course	PG 76-28	11.5	100	98	60	4
	Binder Course	PG 76-28	9.5	100	77	65	4
	Base Course	PG 64-22	9.1	100	77	65	4

Project Name	Pavement Layer	Binder Grade	Binder Content	Gradation			
				3/4″	3/8″	#4	#200
027K0015600-EB	Surface Course	PG 70-28	11.9	100	96	71	5
	Binder Course	PG 70-28	10.3	98	79	68	4
	Base Course	PG 64-22	10.1	98	76	65	3
Project Name	Pavement Layer	Binder Grade	Binder Content	Gradation			
				3/4″	3/8″	#4	#200
028U0005000-EB	Surface Course	PG 70-28	11.8	100	94	70	4
	Binder Course	PG 64-22	11	98	83	72	3
	Base Course	PG 64-22	11	99	82	66	4
Project Name	Pavement Layer	Binder Grade	Binder Content	Gradation			
				3/4″	3/8″	#4	#200
031K0001800-WB	Surface Course	PG 70-28	11.8	100	99	72	5
	Binder Course	PG 70-28	9.6	98	84	67	2
	Base Course	PG 64-22	9.6	98	83	67	2
Project Name	Pavement Layer	Binder Grade	Binder Content	Gradation			
				3/4″	3/8″	#4	#200
033U0028300-NB	Surface Course	PG 64-28	11.7	100	94	74	4
	Binder Course	PG 64-22	10.3	98	67	56	2
	Base Course	PG 64-22	10.3	98	67	56	2
Project Name	Pavement Layer	Binder Grade	Binder Content	Gradation			
				3/4″	3/8″	#4	#200
052U0007300-NB	Surface Course	PG 64-28	10.8	100	97	58	3
	Binder Course	PG 64-28	9.5	100	74	59	3
	Base Course	PG 64-22	9.2	100	73	58	3

Project Name	Pavement Layer	Binder Grade	Binder Content	Gradation			
				3/4″	3/8″	#4	#200
065K0002700-NB	Surface Course	PG 58-28	11.9	100	93	53	5
	Binder Course	PG 58-28	9	88	66	50	7
	Base Course	PG 58-28	9	88	66	50	7
Project Name	Pavement Layer	Binder Grade	Binder Content	Gradation			
				3/4″	3/8″	#4	#200
065U0005600-EB	Surface Course	PG 70-28	11.2	100	94	64	4
	Binder Course	PG 64-22	9.2	99	84	64	5
	Base Course	PG 64-22	9.6	99	84	64	5
Project Name	Pavement Layer	Binder Grade	Binder Content	Gradation			
				3/4″	3/8″	#4	#200
069U0028300-NB	Surface Course	PG 64-28	11	100	96	64	6
	Binder Course	PG 64-28	9.1	100	83	65	6
	Base Course	PG 64-28	9.2	100	84	67	6
Project Name	Pavement Layer	Binder Grade	Binder Content	Gradation			
				3/4″	3/8″	#4	#200
082U0018300-NB	Surface Course	PG 64-28	12.3	100	96	71	4
	Binder Course	PG 64-28	10.3	97	81	67	5
	Base Course	PG 64-28	10.1	97	80	69	4
Project Name	Pavement Layer	Binder Grade	Binder Content	Gradation			
				3/4″	3/8″	#4	#200
095U0005600-EB	Surface Course	PG 70-28	13.1	100	97	79	5
	Binder Course	PG 64-22	10.5	99	82	66	5
	Base Course	PG 70-28	9.9	98	81	65	5

Project Name	Pavement Layer	Binder Grade	Binder Content	Gradation			
				3/4″	3/8″	#4	#200
022K0000700-NB	Surface Course	PG 64-28	11.6	100	98	78	3
	Binder Course	PG 64-28	9.8	100	71	56	5
	Base Course	PG 64-22	9.9	100	80	63	3
Project Name	Pavement Layer	Binder Grade	Binder Content	Gradation			
				3/4″	3/8″	#4	#200
025K0009900-NB	Surface Course	PG 64-28	12.9	100	95	72	2
	Binder Course	PG 64-22	10.3	98	67	56	2
	Base Course	PG 64-28	9.8	97	69	56	3
Project Name	Pavement Layer	Binder Grade	Binder Content	Gradation			
				3/4″	3/8″	#4	#200
003U0007300-NB	Surface Course	PG 64-28	10.9	100	97	61	4
	Binder Course	PG 64-28	9.4	100	72	56	4
	Base Course	PG 64-22	9.3	100	73	58	3
Project Name	Pavement Layer	Binder Grade	Binder Content	Gradation			
				3/4″	3/8″	#4	#200
022K0000700-NB	Surface Course	PG 64-28	11.6	100	98	78	3
	Binder Course	PG 64-28	9.8	100	71	56	5
	Base Course	PG 64-22	9.9	100	80	63	3
Project Name	Pavement Layer	Binder Grade	Binder Content	Gradation			
				3/4″	3/8″	#4	#200
088U0005400-WB	Surface Course	PG 70-28	10.9	100	94	71	4
	Binder Course	PG 70-28	9.6	98	82	68	4
	Base Course	PG 64-22	9.8	97	81	66	4

Project Name	Pavement Layer	Binder Grade	Binder Content	Gradation			
				3/4″	3/8″	#4	#200
091K0002700-NB	Surface Course	PG 64-28	13.6	100	98	84	6
	Binder Course	PG 64-28	9.7	98	76	59	5
	Base Course	PG 64-22	9.7	98	73	54	3
Project Name	Pavement Layer	Binder Grade	Binder Content	Gradation			
				3/4″	3/8″	#4	#200
098U0028300-NB	Surface Course	PG 64-28	11.9	100	97	75	4
	Binder Course	PG 64-28	10.9	95	82	57	4
	Base Course	PG 64-22	10.5	99	80	71	4
Project Name	Pavement Layer	Binder Grade	Binder Content	Gradation			
				3/4″	3/8″	#4	#200
103K0003900-NB	Surface Course	PG 64-28	10.7	100	98	67	5
	Binder Course	PG 64-28	8.7	99	79	61	4
	Base Course	PG 64-28	8.7	99	79	61	5

Table A 3. Site-specific subgrade soil properties for new flexible pavements

Project No.	County	Soil Type	Gradation (% Passing)				Atterberg Limits	
			#4 Sieve	#10 Sieve	#40 Sieve	#200 Sieve	Liquid Limit	Plasticity Index
003U0007300-NB	Atchison	Sharpsburg Silty Clay Loam	100	100	100	95-100	40-60	20-35
007U0007500-NB	Brown	Judson Silt Loam	100	100	100	95-100	30-50	15-25
008U0007700-NB-1	Butler	Ladysmith Silt Clay Loam	100	100	95-100	95-100	47	27
008U0007700-NB-2	Butler	Verdigris Silt Loam	100	100	95-100	95-100	47	27
008U0007700-NB-3	Butler	Labette-Dwight complex Silt Loam	100	100	95-100	95-100	47	27
008U0005400-EB	Butler	Verdigris Silt Loam	100	100	95-100	90-100	52	29
011U0006900-NB	Cherokee	Labette-Dwight complex Silt Loam	100	100	95-100	90-100	47	27
019K0000700-NB-1	Crawford	Parsons Silt Loam	100	100	95-100	85-95	49	30
019K0000700-NB-2	Crawford	Lula Silt Loam	100	100	98	91	57	32
019U0016000-EB	Crawford	Lula-Clareson complex	100	100	98	91	57	32
022K0000700-NB	Doniphan	Monona silt loam	100	100	95-100	95-100	30-45	10-20
023U0004000-EB	Douglas	Martin silts clay loam	100	100	95-100	80-98	41-70	25-40
025K0009900-NB	Elk	Kenoma silt loam	85-100	85-100	75-100	75-95	45-65	25-44
027K0015600-EB	Ellsworth	Crete silt loam	100	100	100	95-100	30-55	10-35
028U0005000-EB	Finney	Ulysses silt loam	100	100	100	90-100	30-55	10-35
031K0001800-WB	Geary	Muir silt clay loam	100	100	95-100	90-100	-	-
033U0028300-NB	Graham	Holdrege silt loam	100	100	95-100	95-100	25-40	9-17

Project No.	County	Soil Type	Gradation (% Passing)				Atterberg Limits	
			#4 Sieve	#10 Sieve	#40 Sieve	#200 Sieve	Liquid Limit	Plasticity Index
052U0007300-NB	Leavenworth	Marshall silt loam	100	100	90-100	95-100	44	23
065K0002700-NB	Morton	Dalhart loamy fine sand	92	64	20	9	16	2
065U0005600-EB	Morton	Dalhart loamy fine sand	92	64	20	9	16	2
069U0028300-NB	Norton	Holdrege silt loam	100	100	98-100	95-100	30-45	5-20
082U0018300-NB	Rooks	Harney silt loam	100	100	95-100	85-100	30-40	10-20
084U0028100-NB	Russell	Nibson silt loam	85-95	80-95	60-90	55-90	30-45	10-25
088U0005400-WB	Seward	Richfield silt loam	100	100	100	90-100	30-45	30-45
091K0002700-NB	Sherman	Keith silt loam	100	100	100	85-100	30-45	10-25
095U0005600-EB	Stevens	Ulysses silt loam	100	100	100	90-100	30-55	10-35
098U0028300-NB	Trego	Hord silt loam	100	100	100	85-100	25-40	6-21
103K0003900-NB	Wilson	Hord silt loam	100	100	100	85-100	25-40	6-21

Appendix B - Measured Versus Predicted data

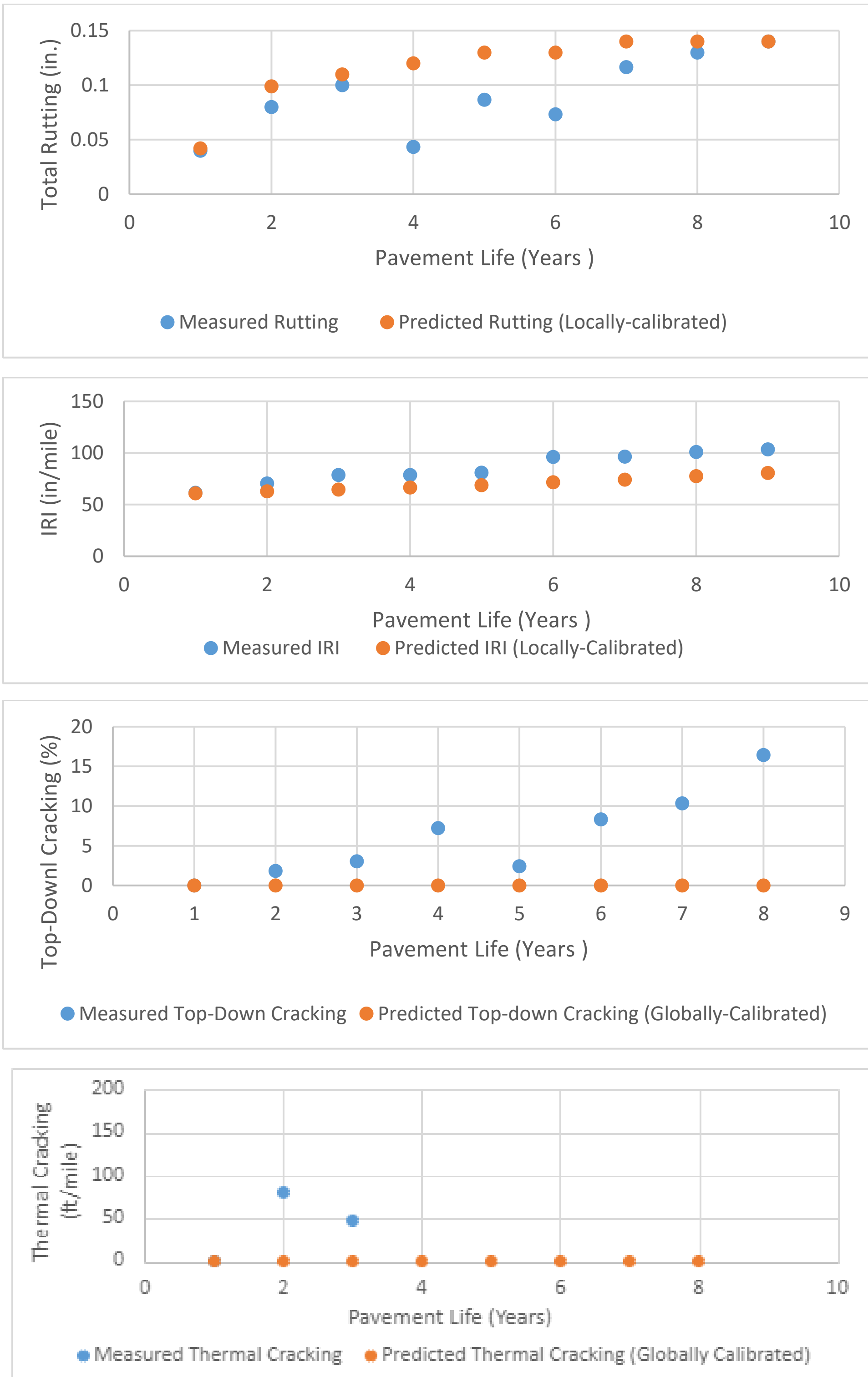

Figure B- 1. Measured and Predicted Performance Data for Project 003U0007300-NB

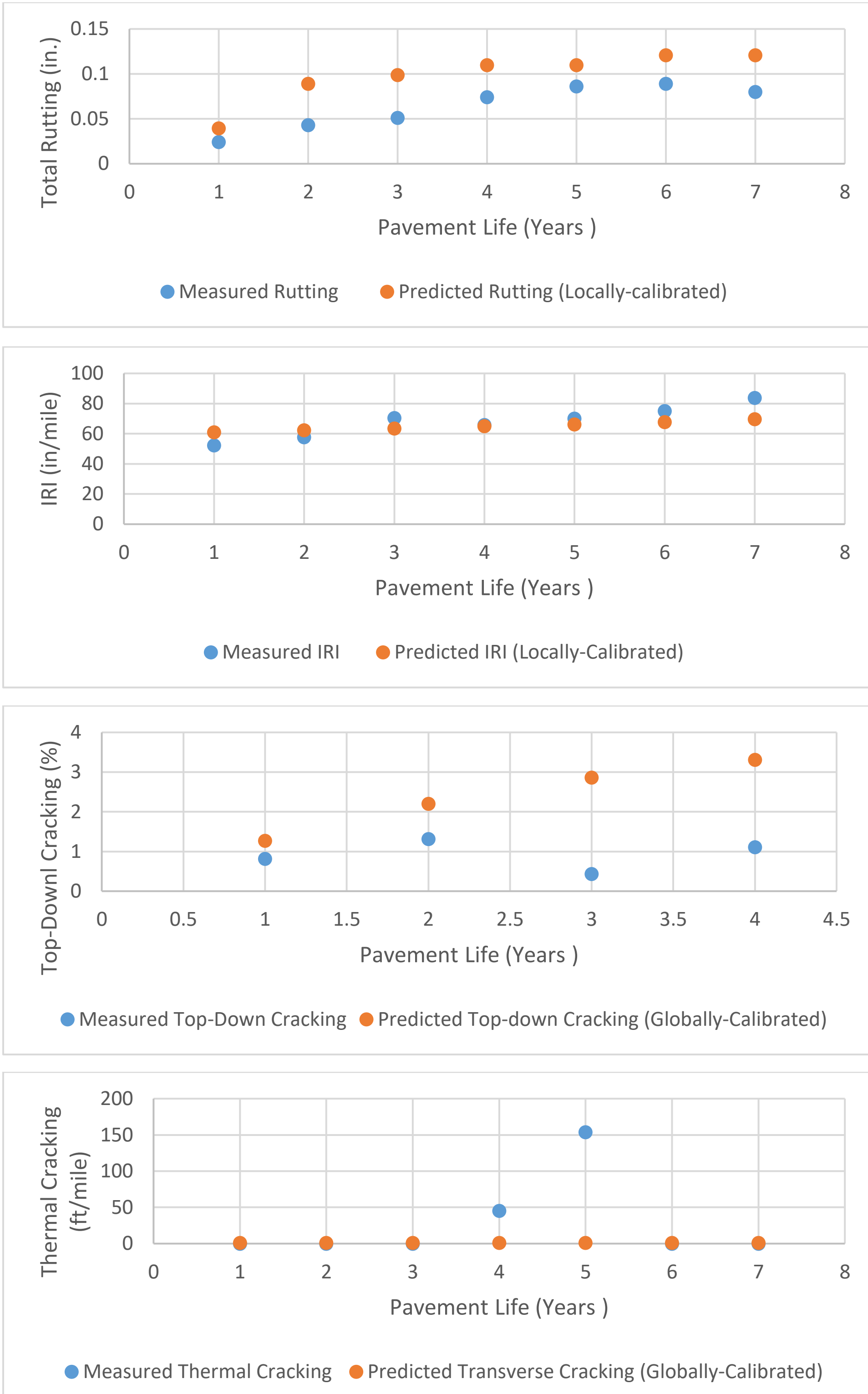

Figure B- 2. Measured and Predicted Performance Data for Project 007U0007500-NB

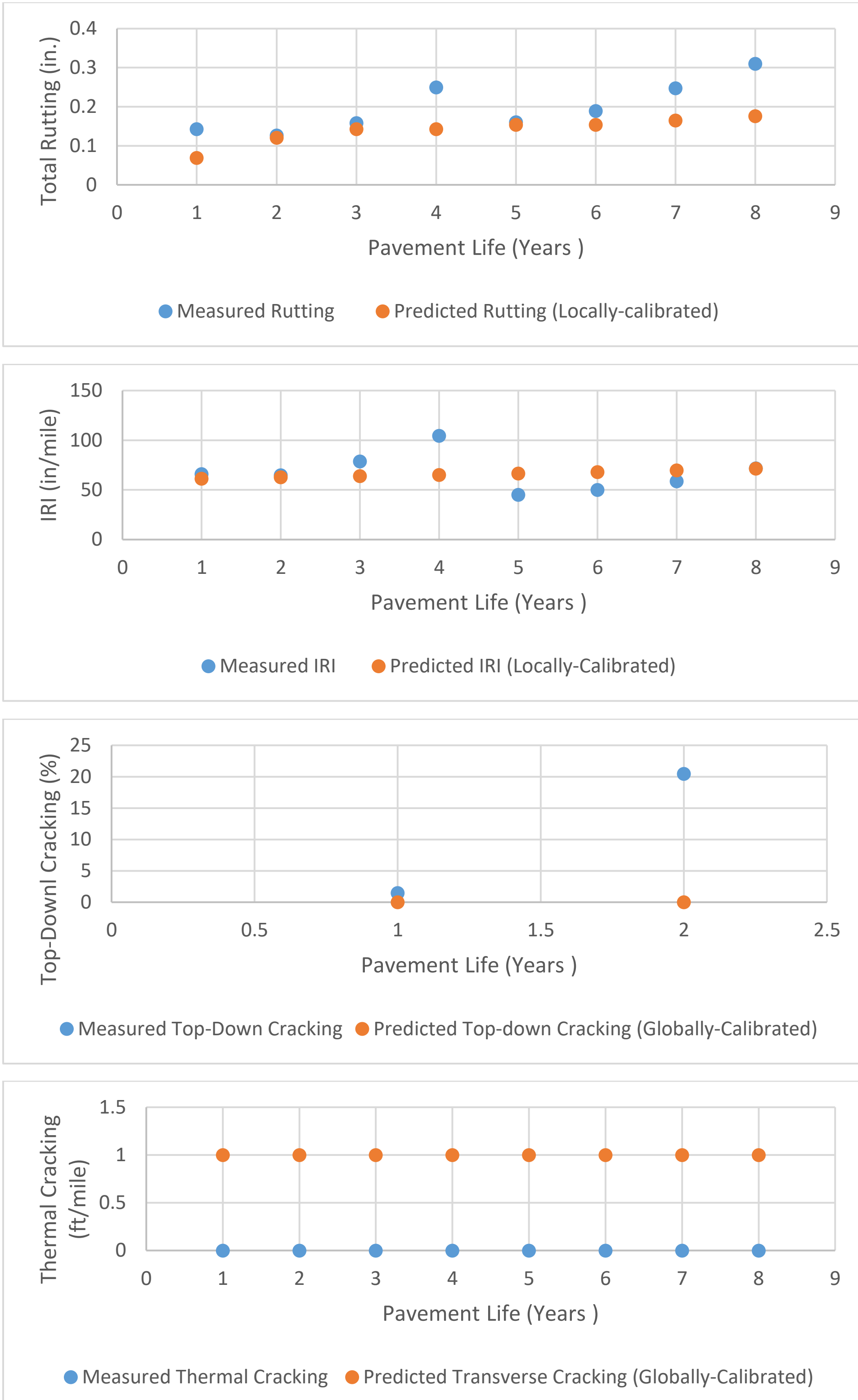

Figure B- 3. Measured and Predicted Performance Data for Project 008U0007700-NB-1

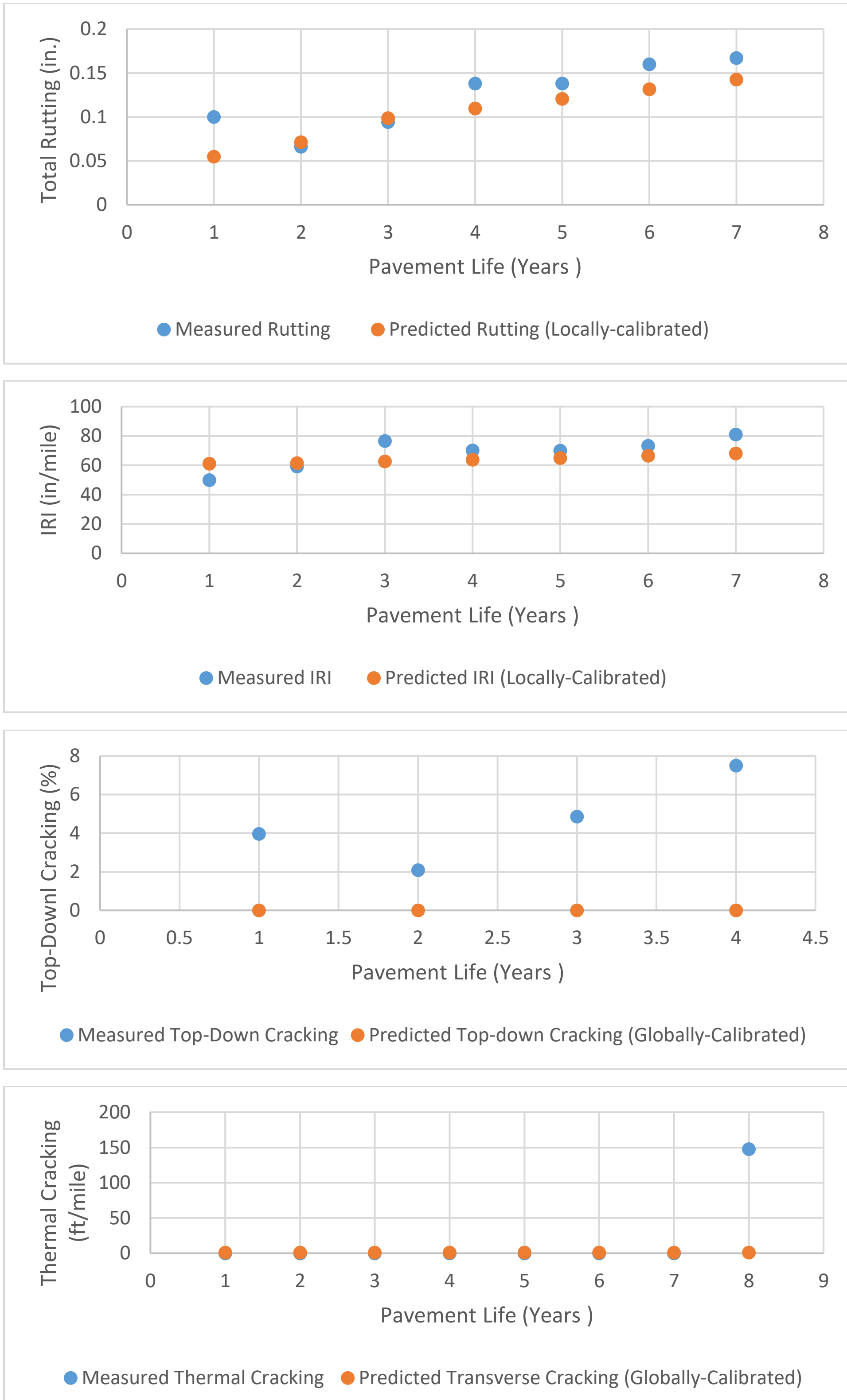

Figure B- 4. Measured and Predicted Performance Data for Project 008U0007700-NB-2

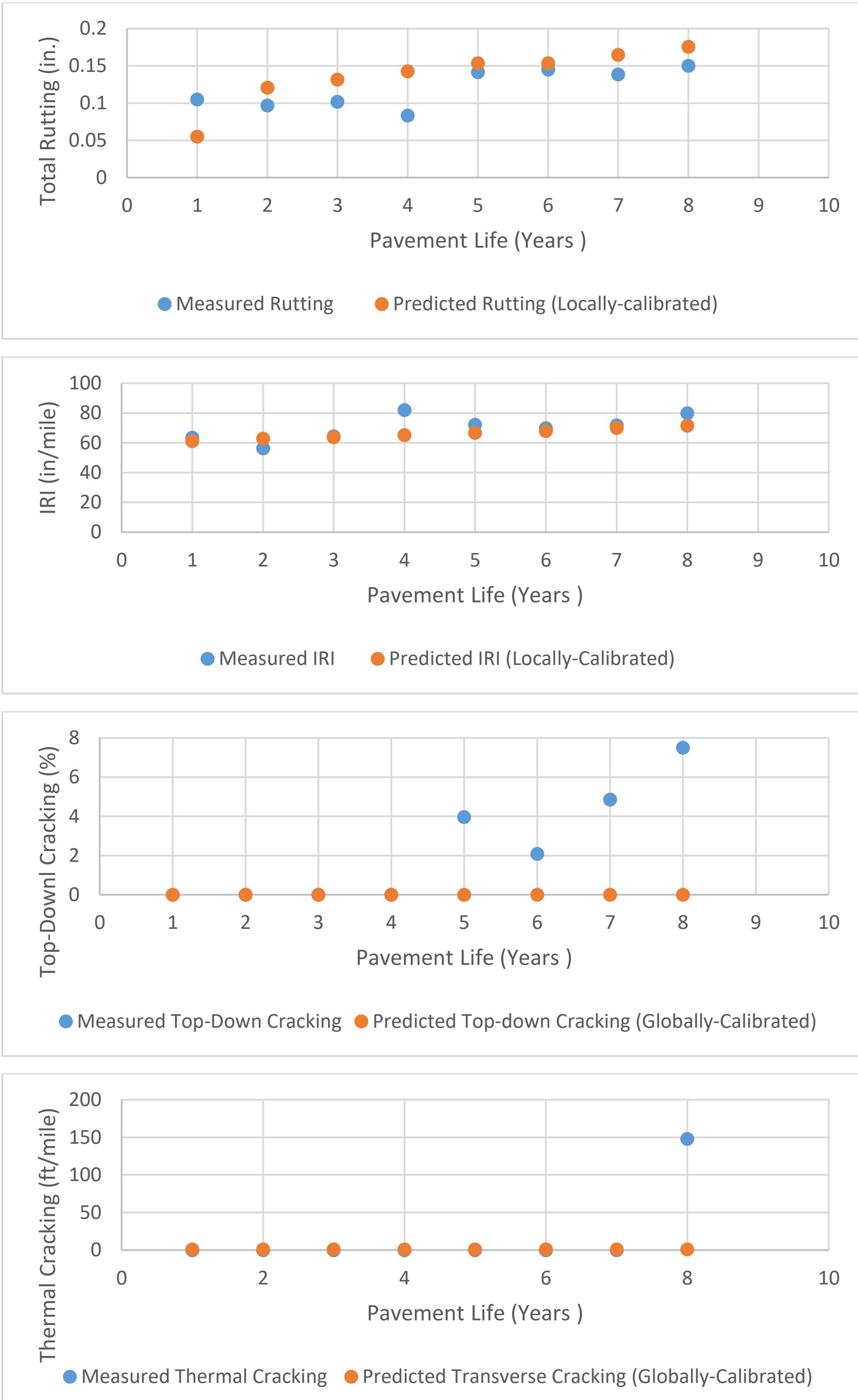

Figure B- 5. Measured and Predicted Performance Data for Project 008U0007700-NB-3

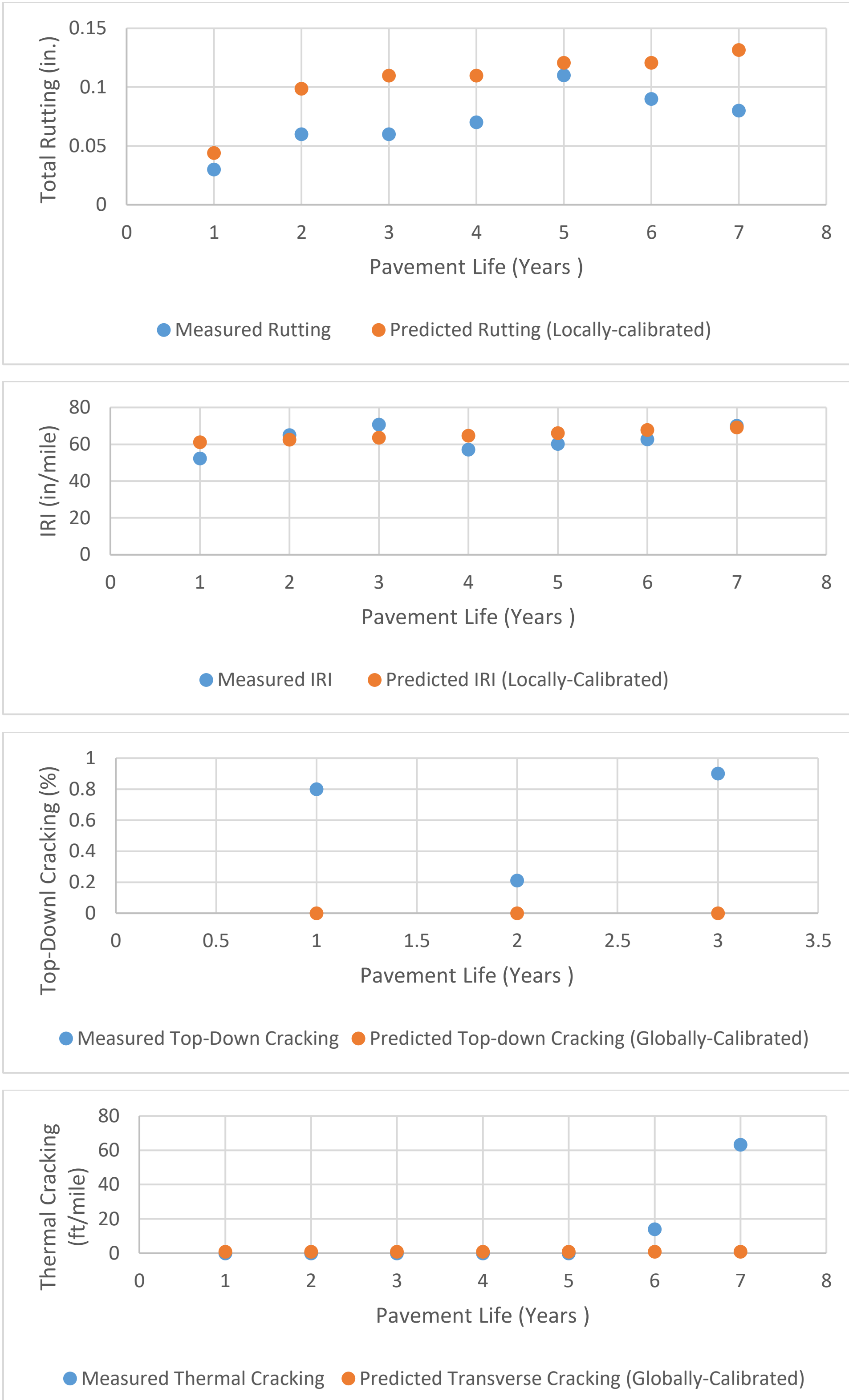

Figure B- 6. Measured and Predicted Performance Data for Project 008U0005400-EB

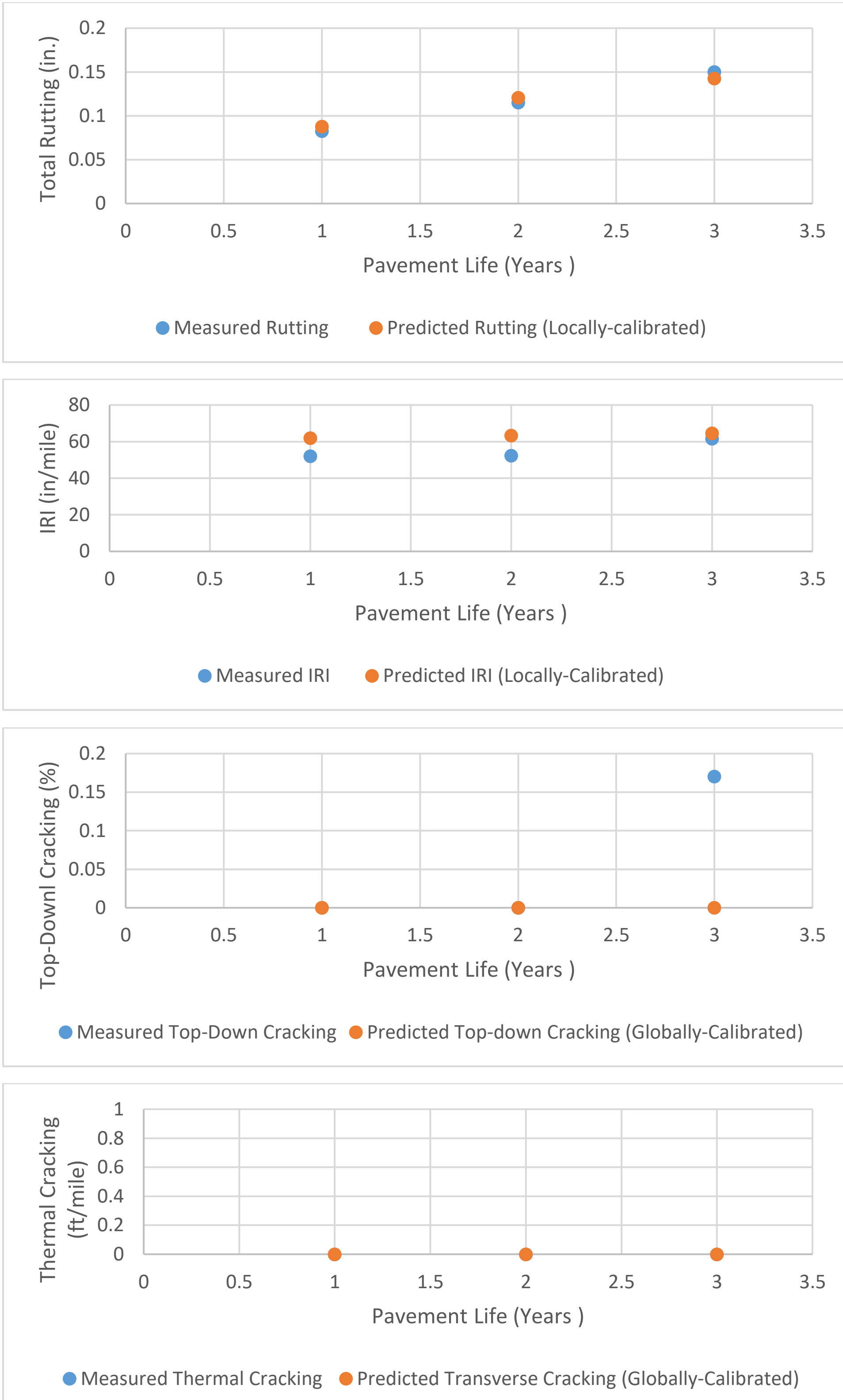

Figure B- 7. Measured and Predicted Performance Data for Project 011U0006900-NB

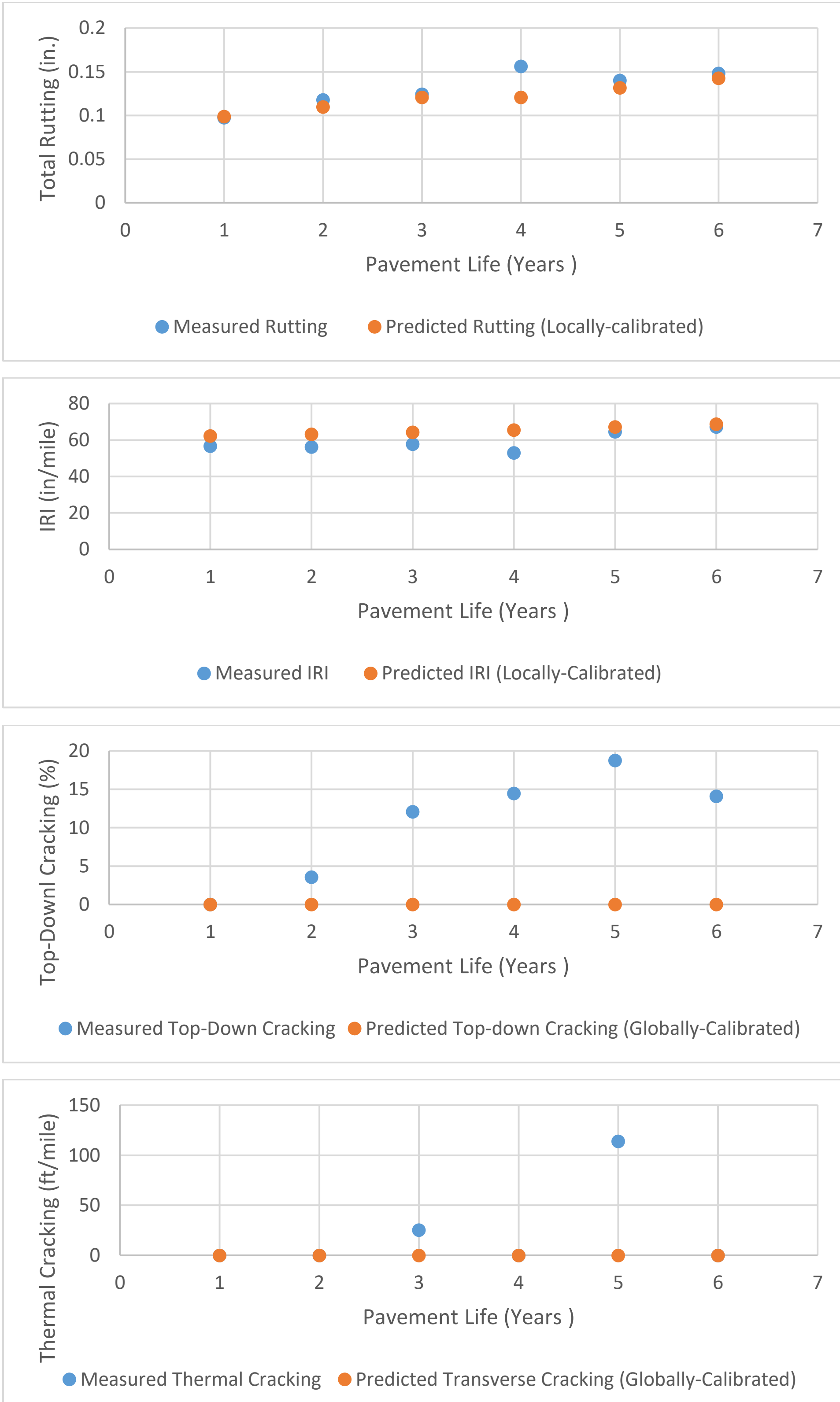

Figure B- 8. Measured and Predicted Performance Data for Project 019K0000700-NB-1

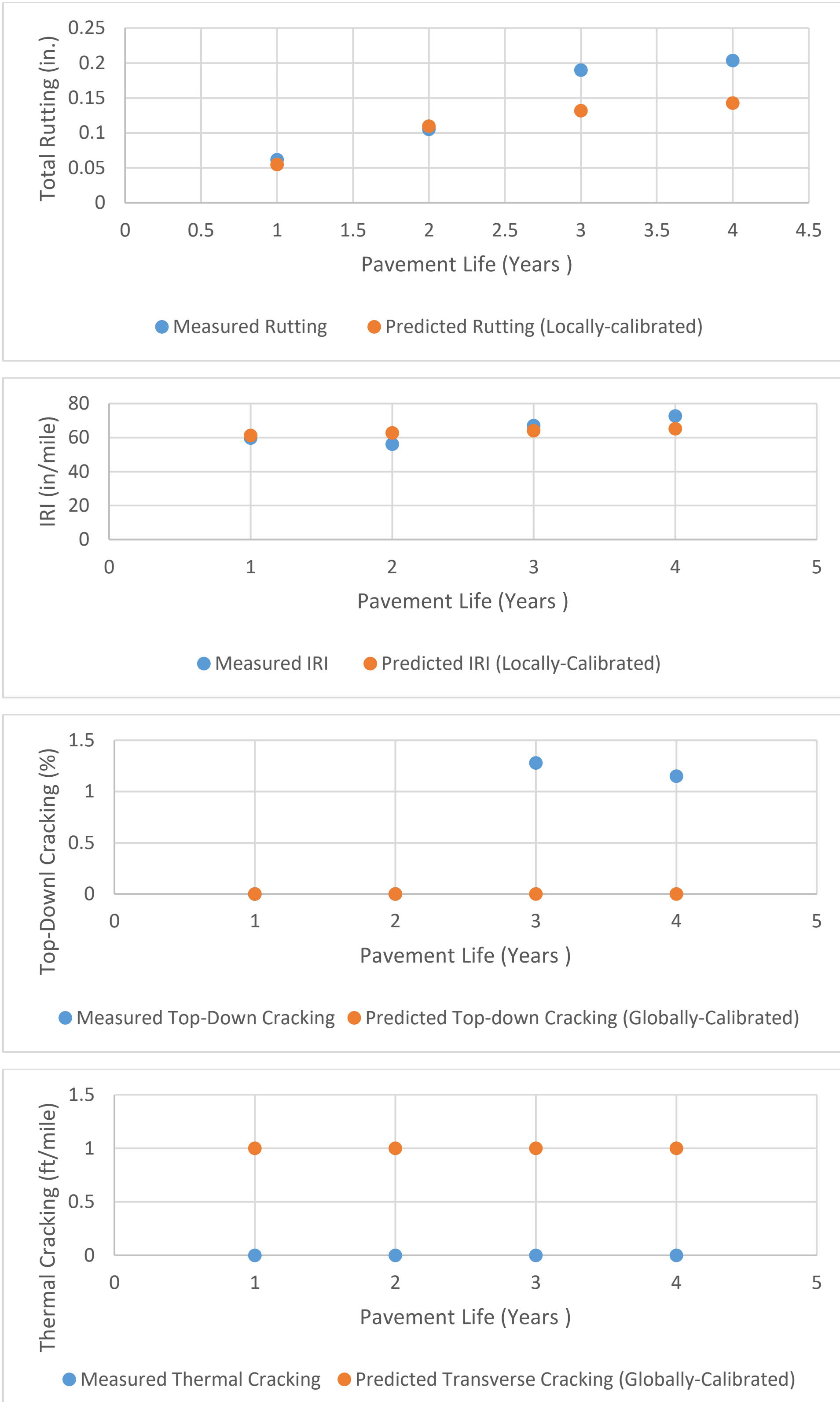

Figure B- 9. Measured and Predicted Performance Data for Project 019K0000700-NB-2

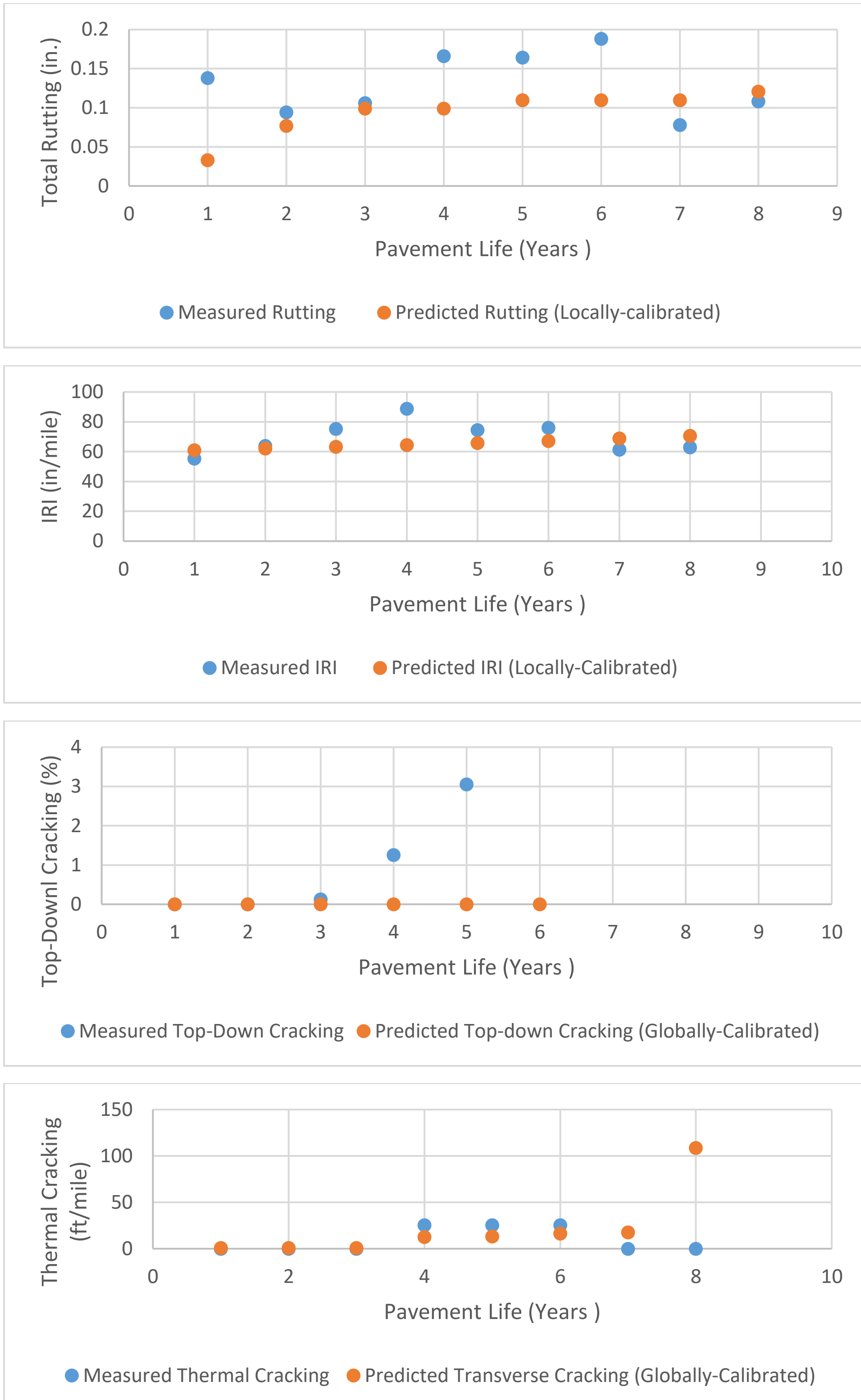

Figure B- 10. Measured and Predicted Performance Data for Project 019U0016000-EB

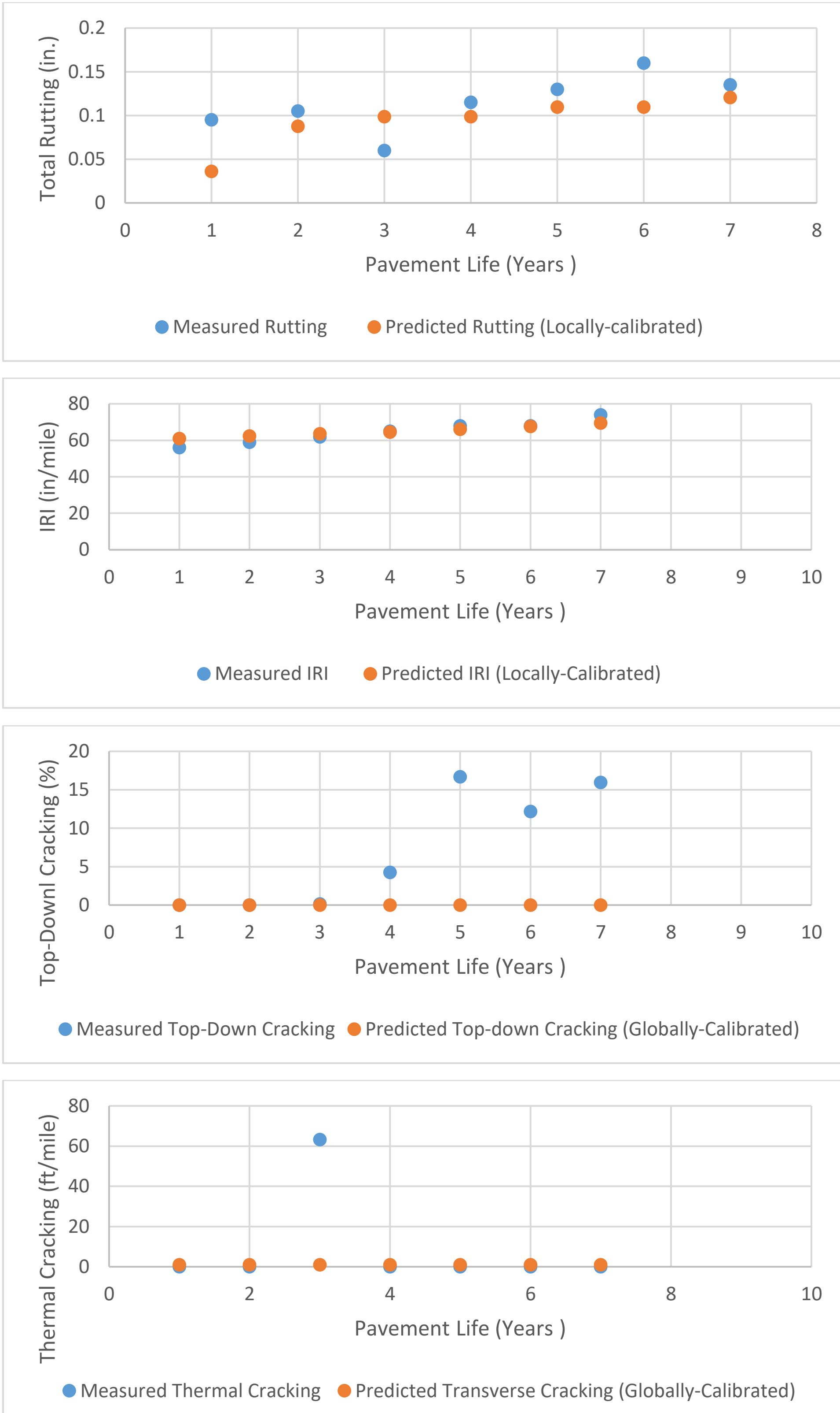

Figure B- 11. Measured and Predicted Performance Data for Project 023U0004000-EB

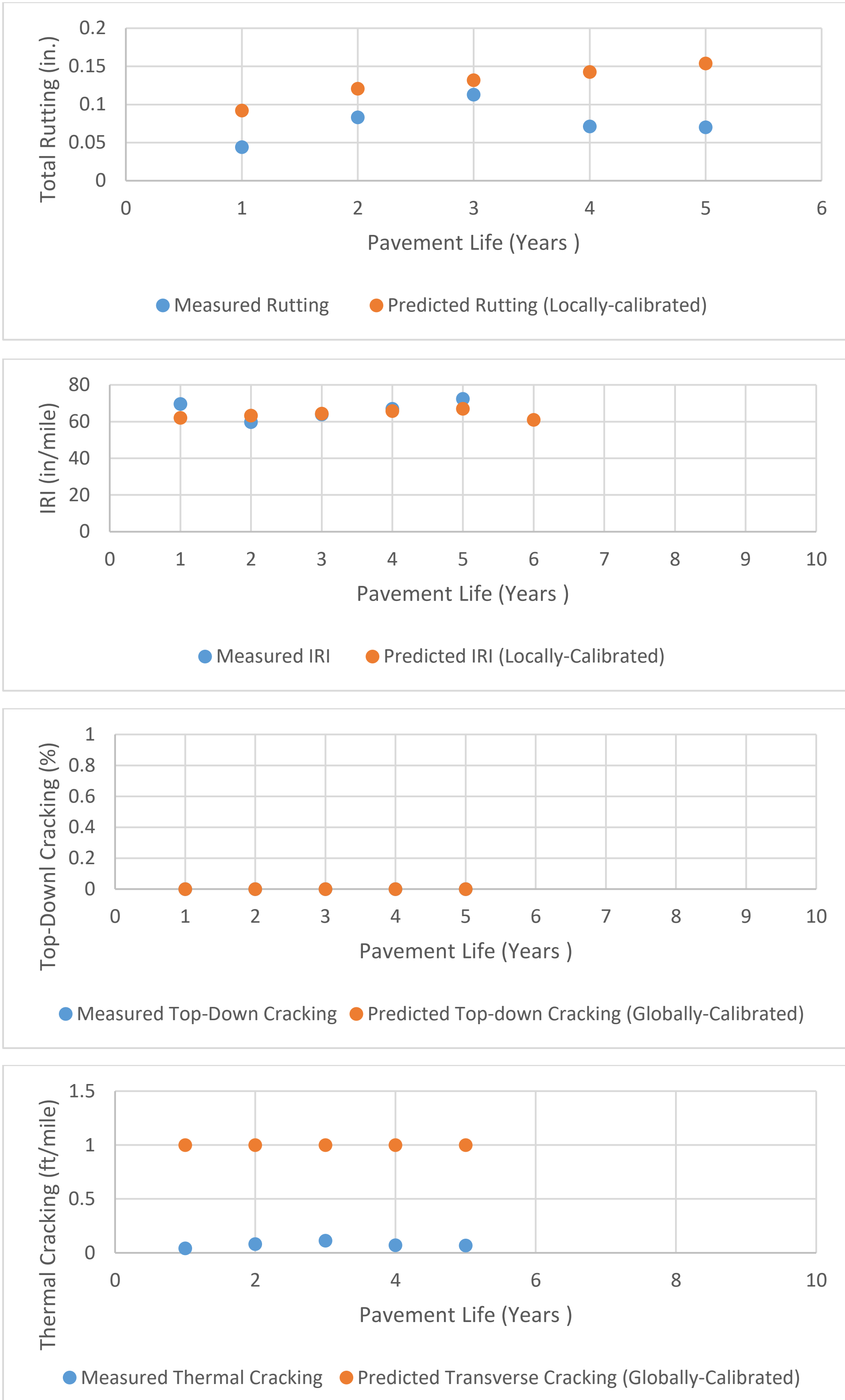

Figure B- 12. Measured and Predicted Performance Data for Project 025K0009900-NB

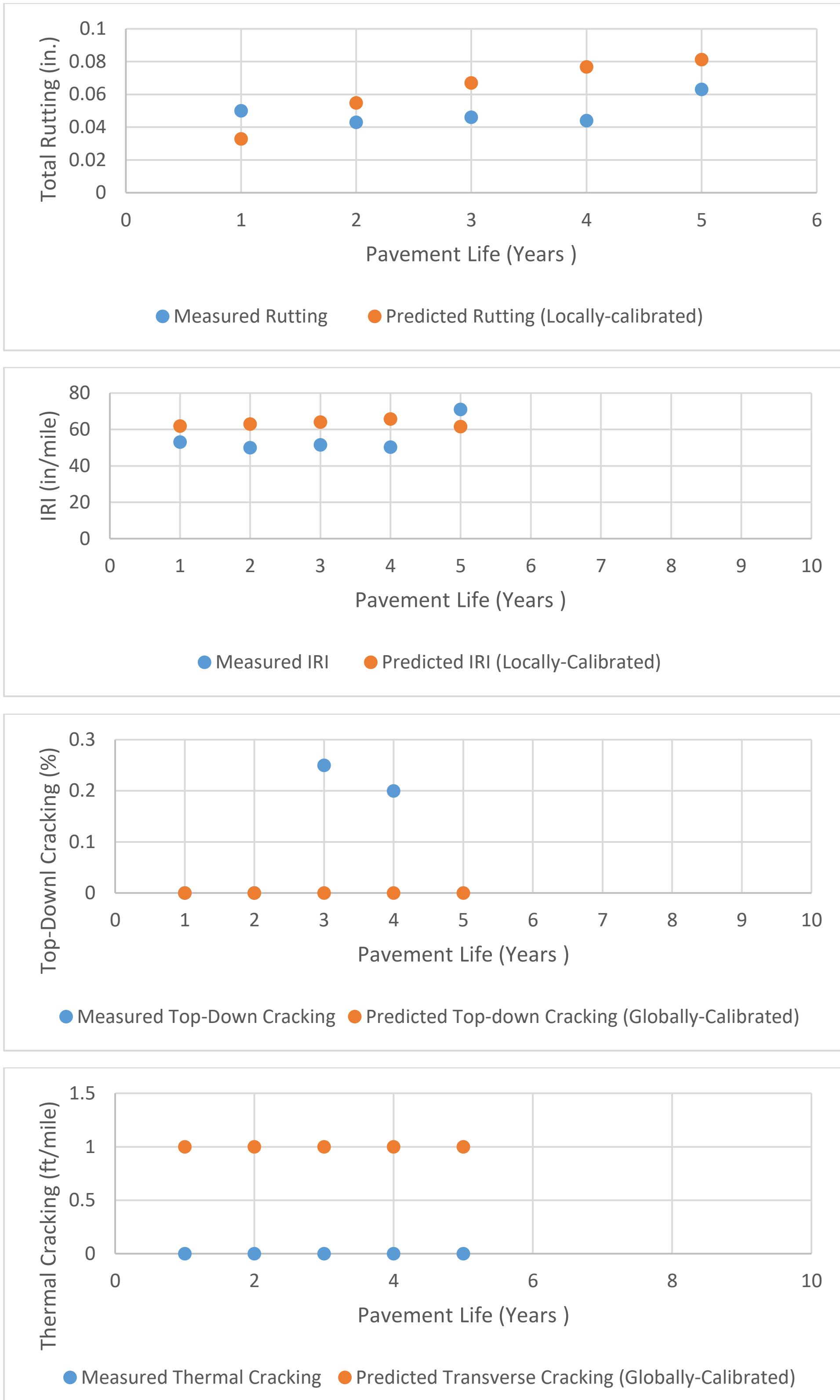

Figure B- 13. Measured and Predicted Performance Data for Project 027K0015600-EB

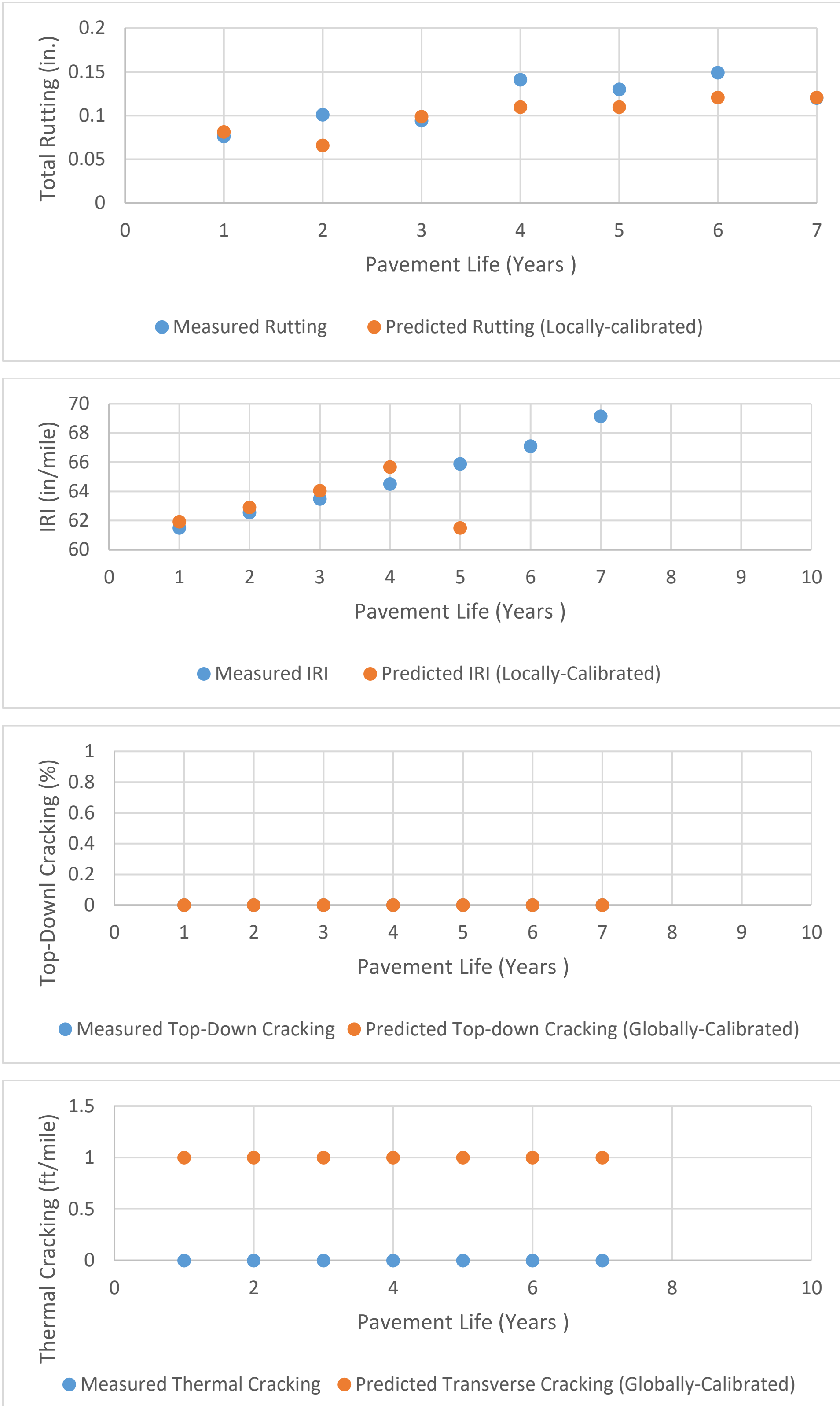

Figure B- 14. Measured and Predicted Performance Data for Project 028U0005000-EB

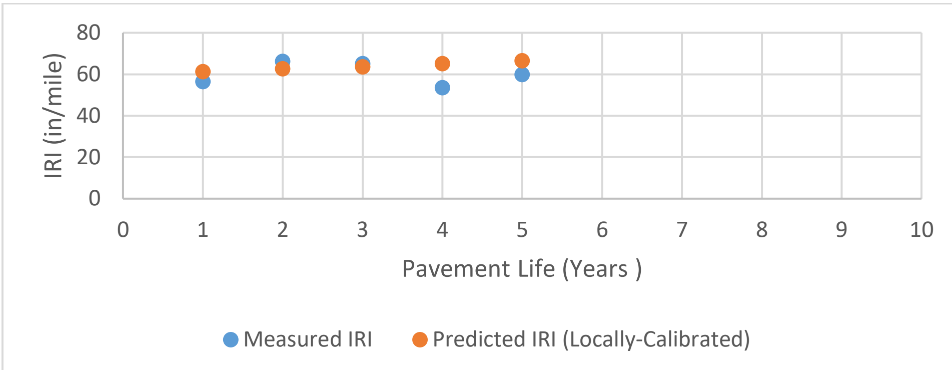

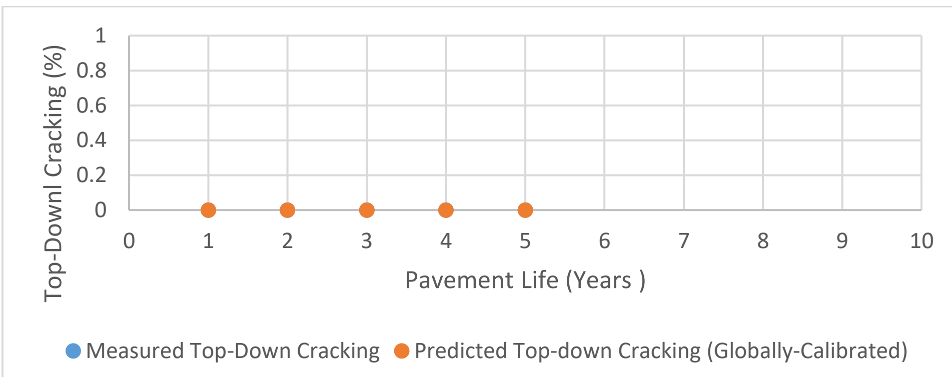

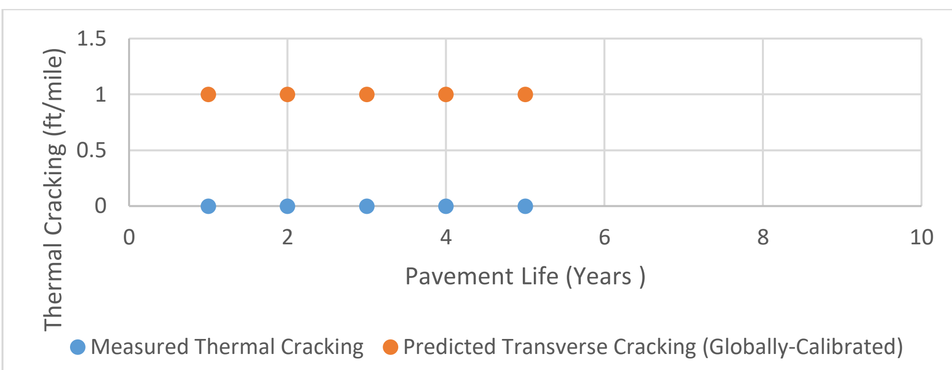

Figure B- 15. Measured and Predicted Performance Data for Project 031K0001800-WB

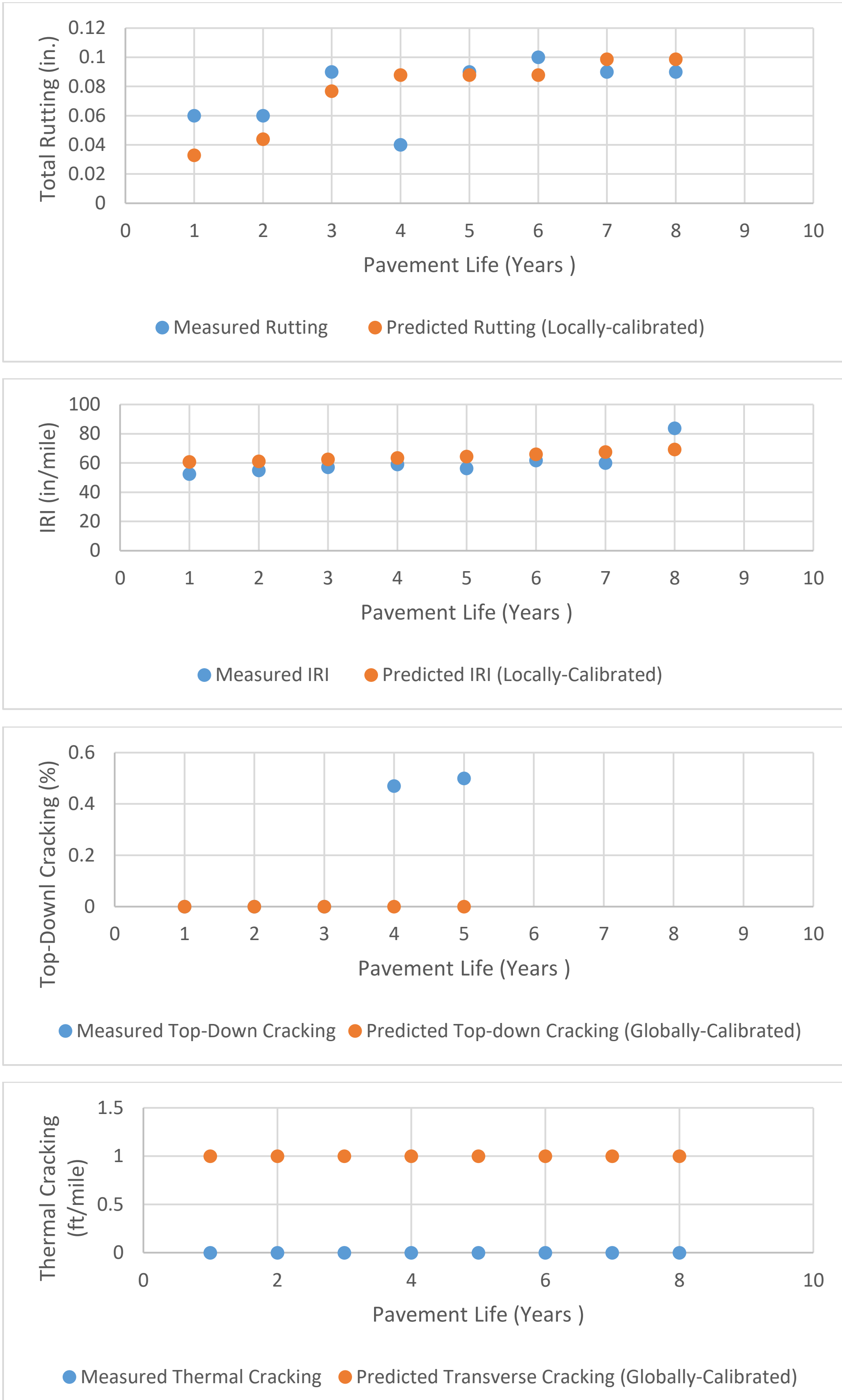

Figure B- 16. Measured and Predicted Performance Data for Project 033U0028300-NB

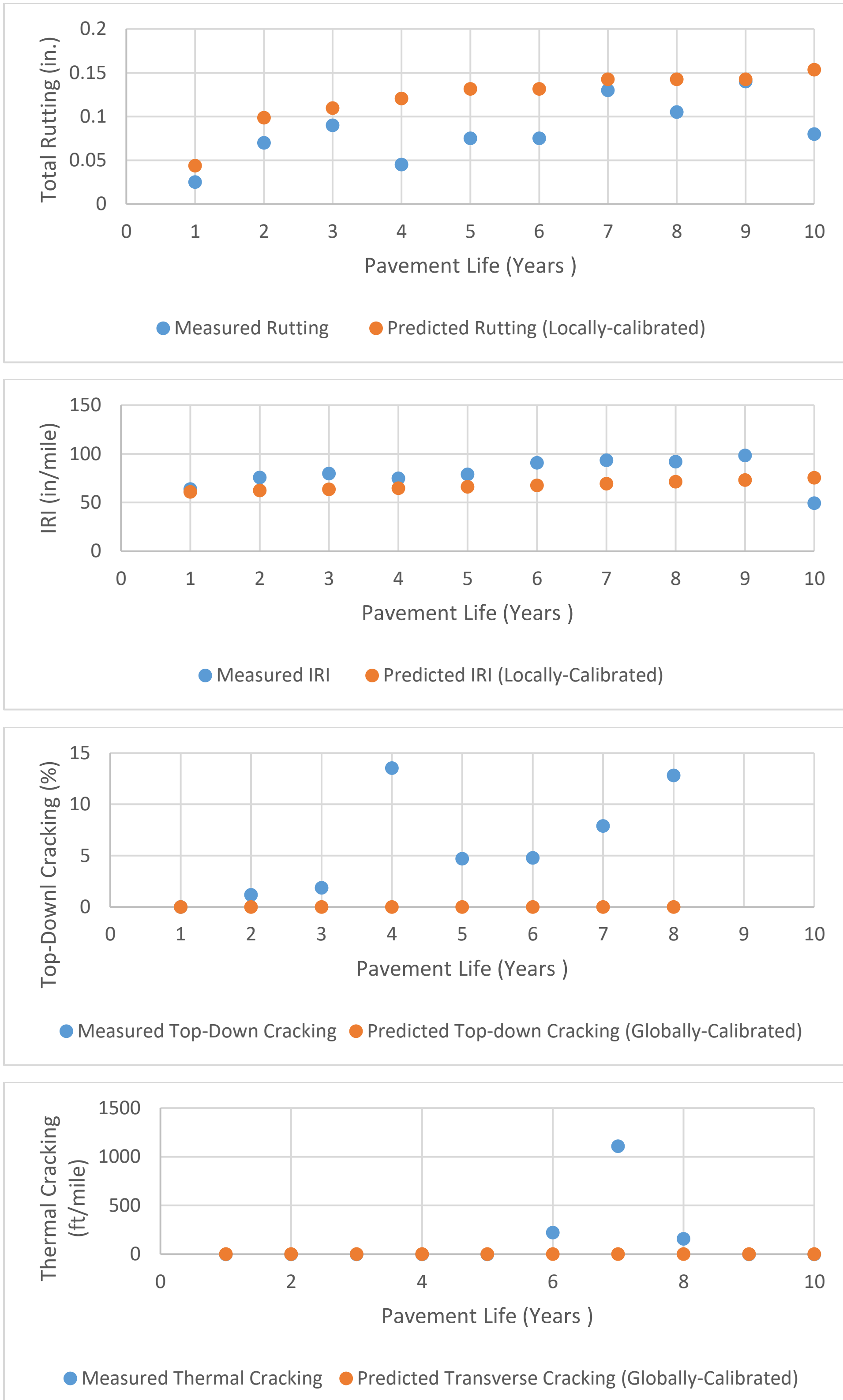

Figure B- 17. Measured and Predicted Performance Data for Project 052U0007300-NB

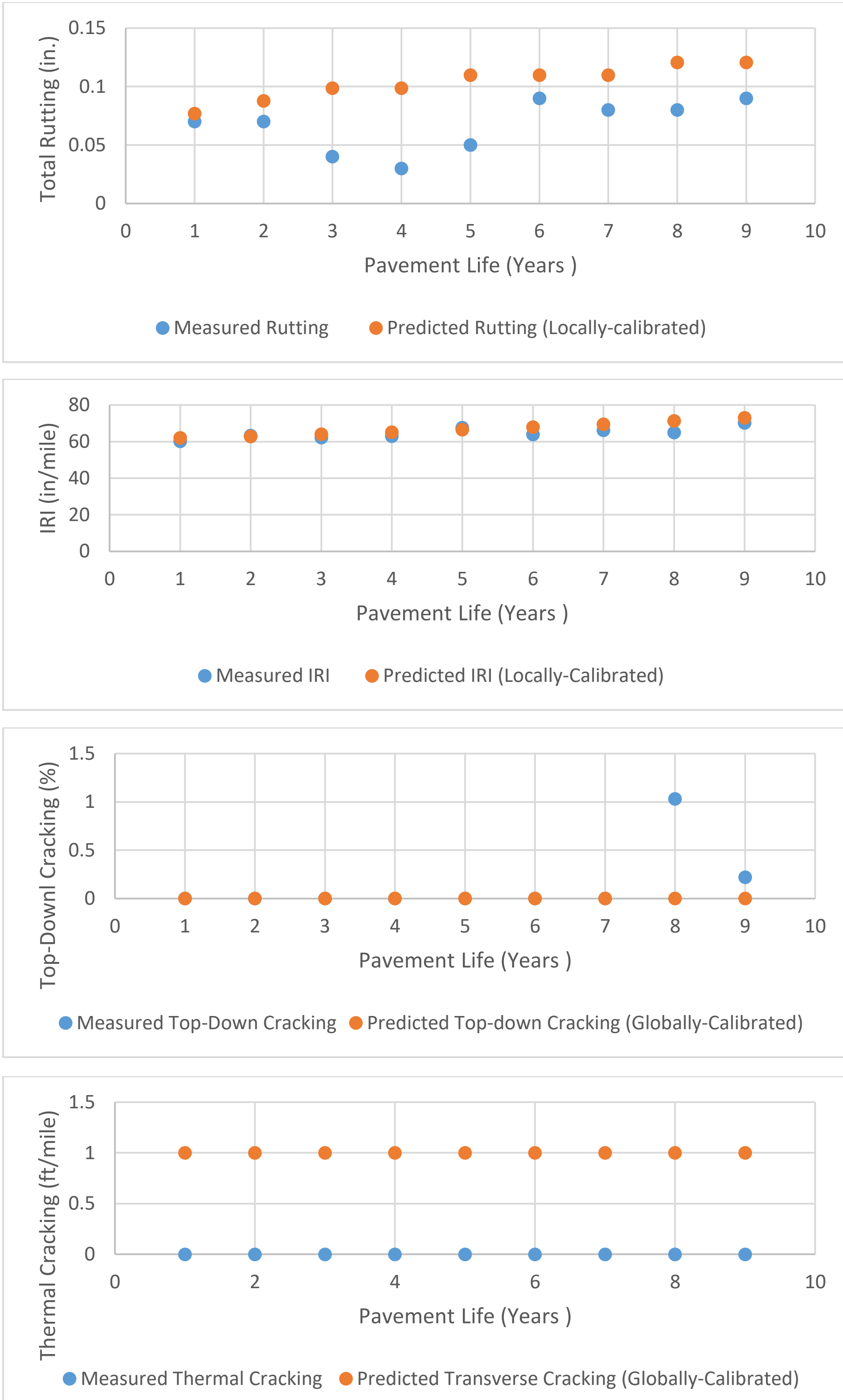

Figure B- 18. Measured and Predicted Performance Data for Project 065K0002700-NB

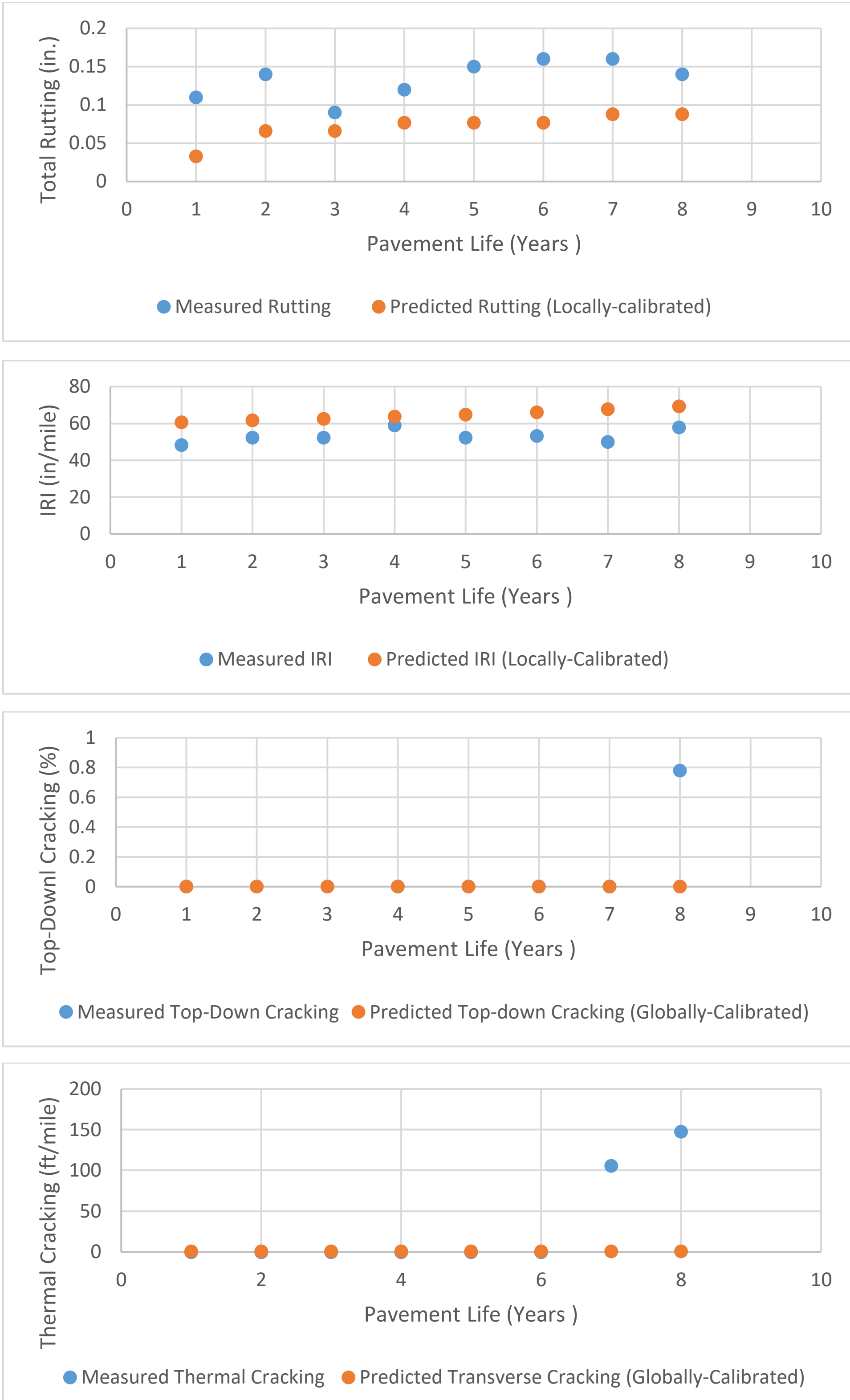

Figure B- 19. Measured and Predicted Performance Data for Project 065U0005600-EB

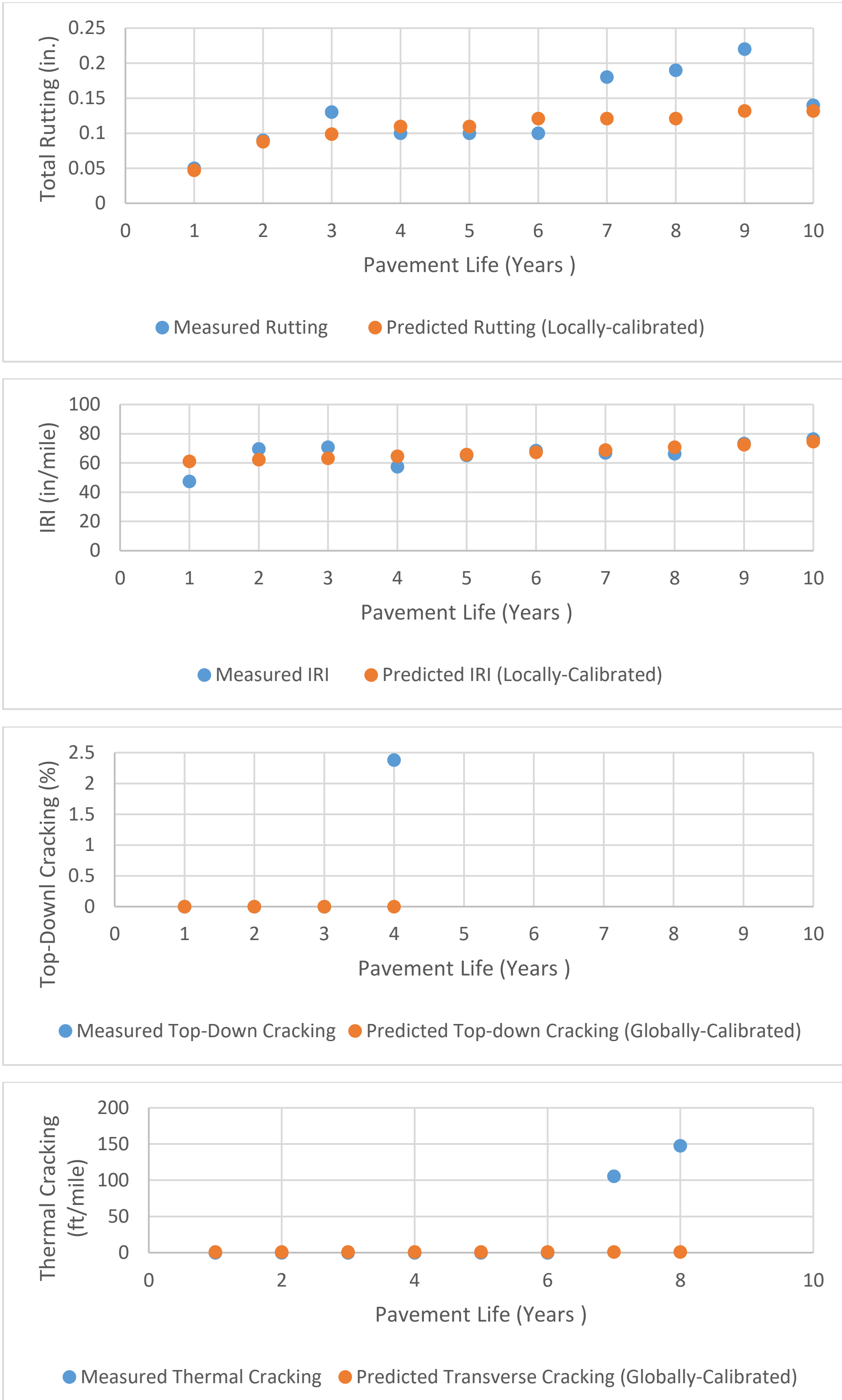

Figure B- 20. Measured and Predicted Performance Data for Project 069U0028300-NB

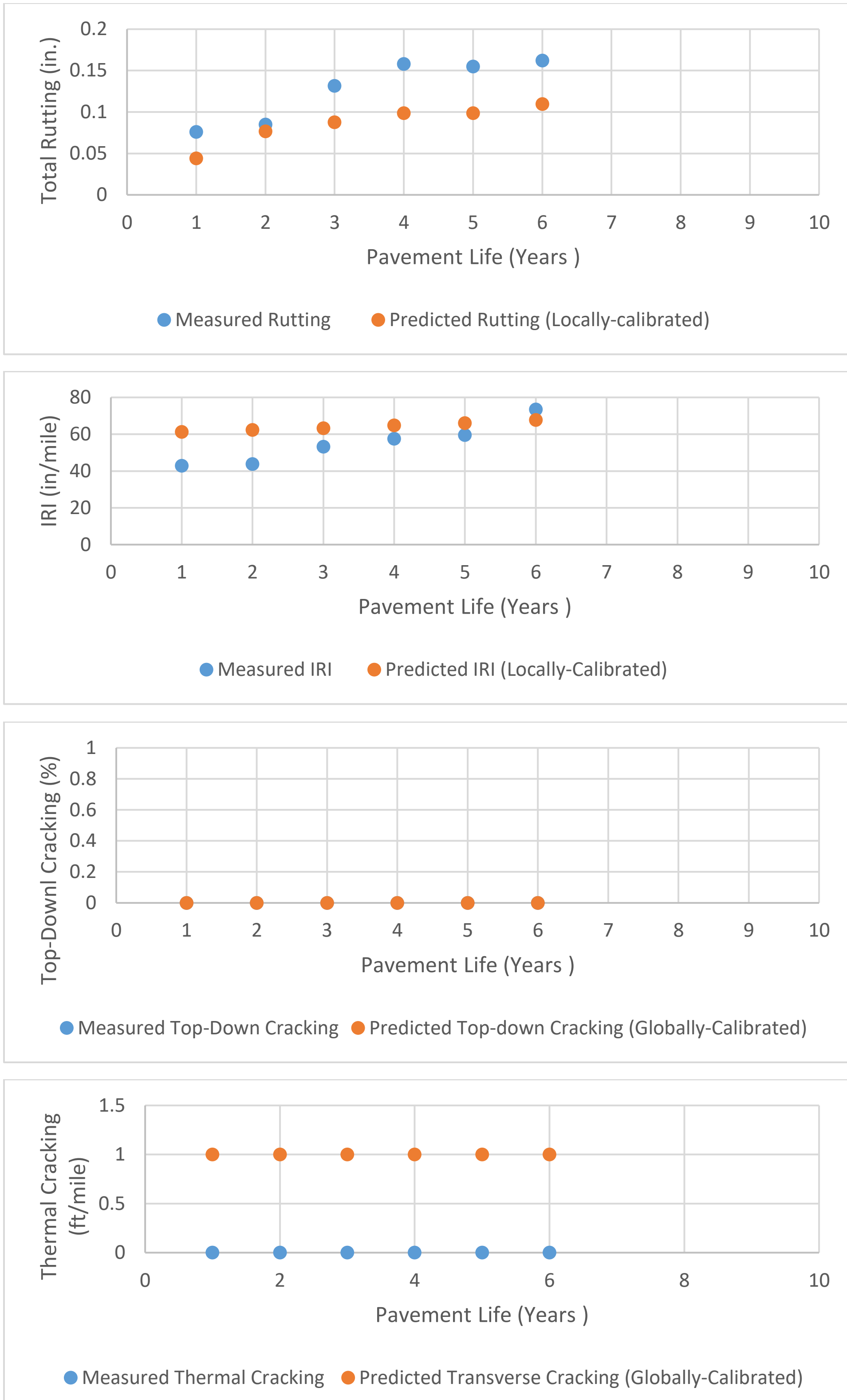

Figure B- 21. Measured and Predicted Performance Data for Project 082U0018300-NB

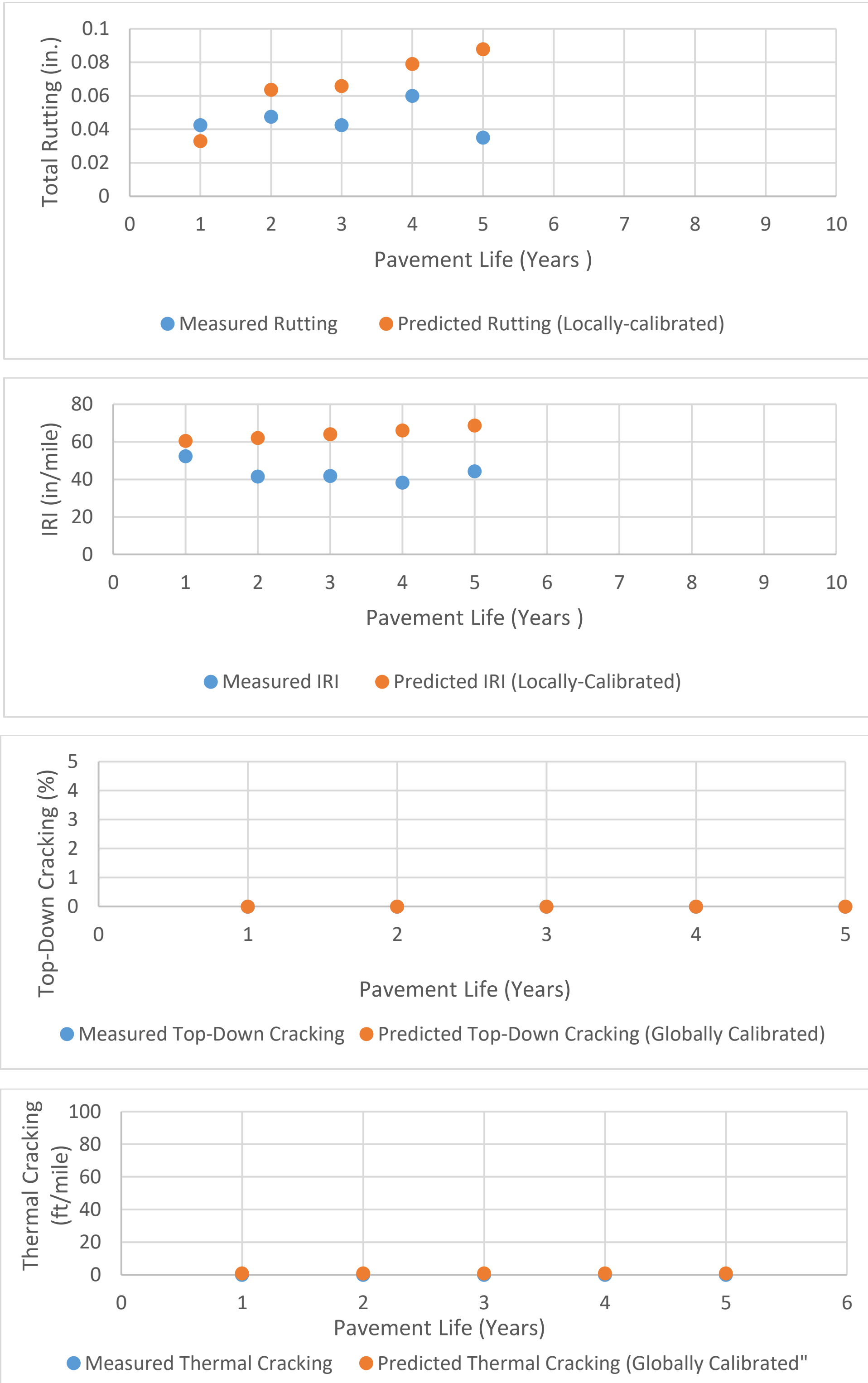

Figure B- 22. Measured and Predicted Performance Data for Project 088U0005400-WB

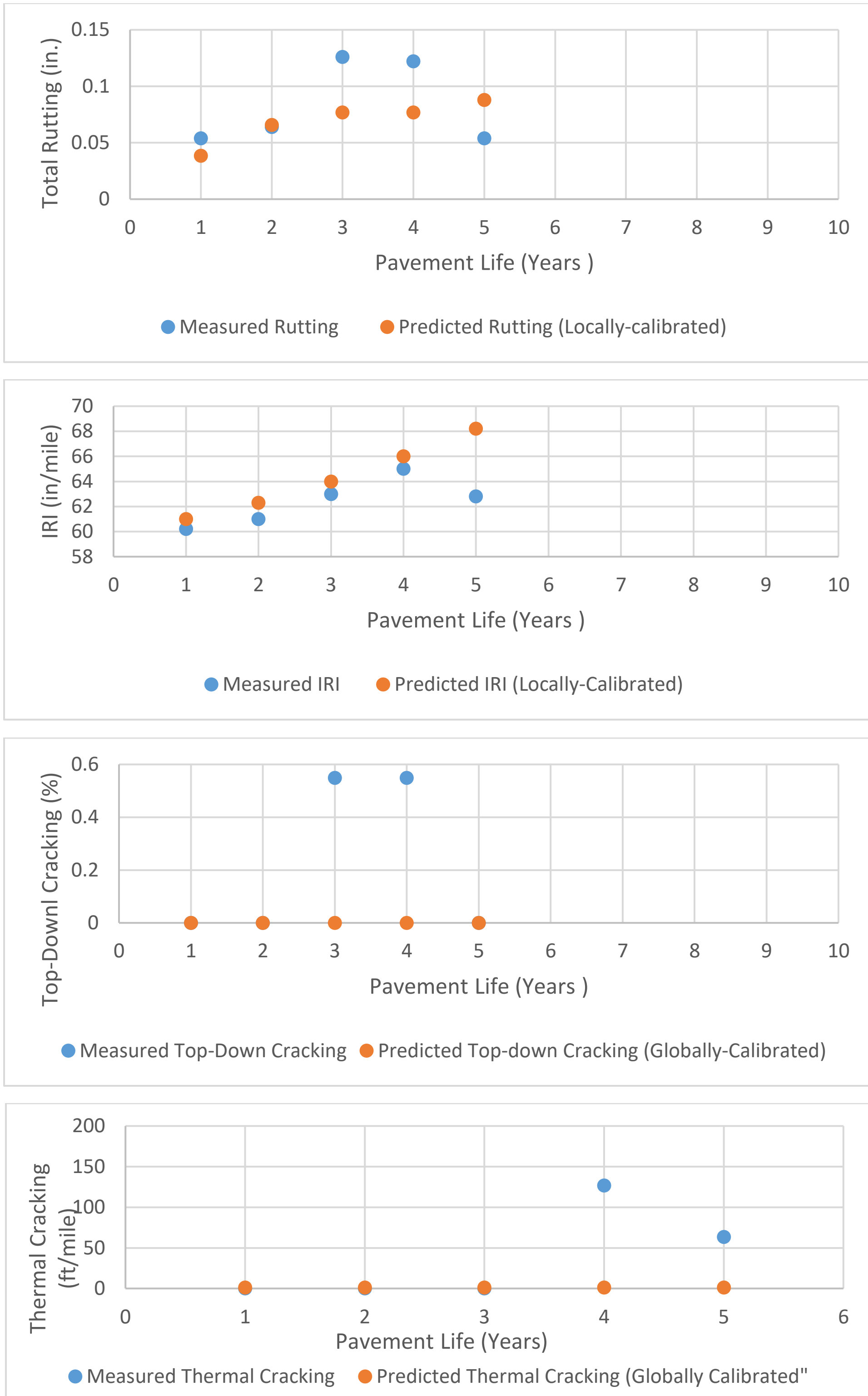

Figure B- 23. Measured and Predicted Performance Data for Project 091K0002700-NB

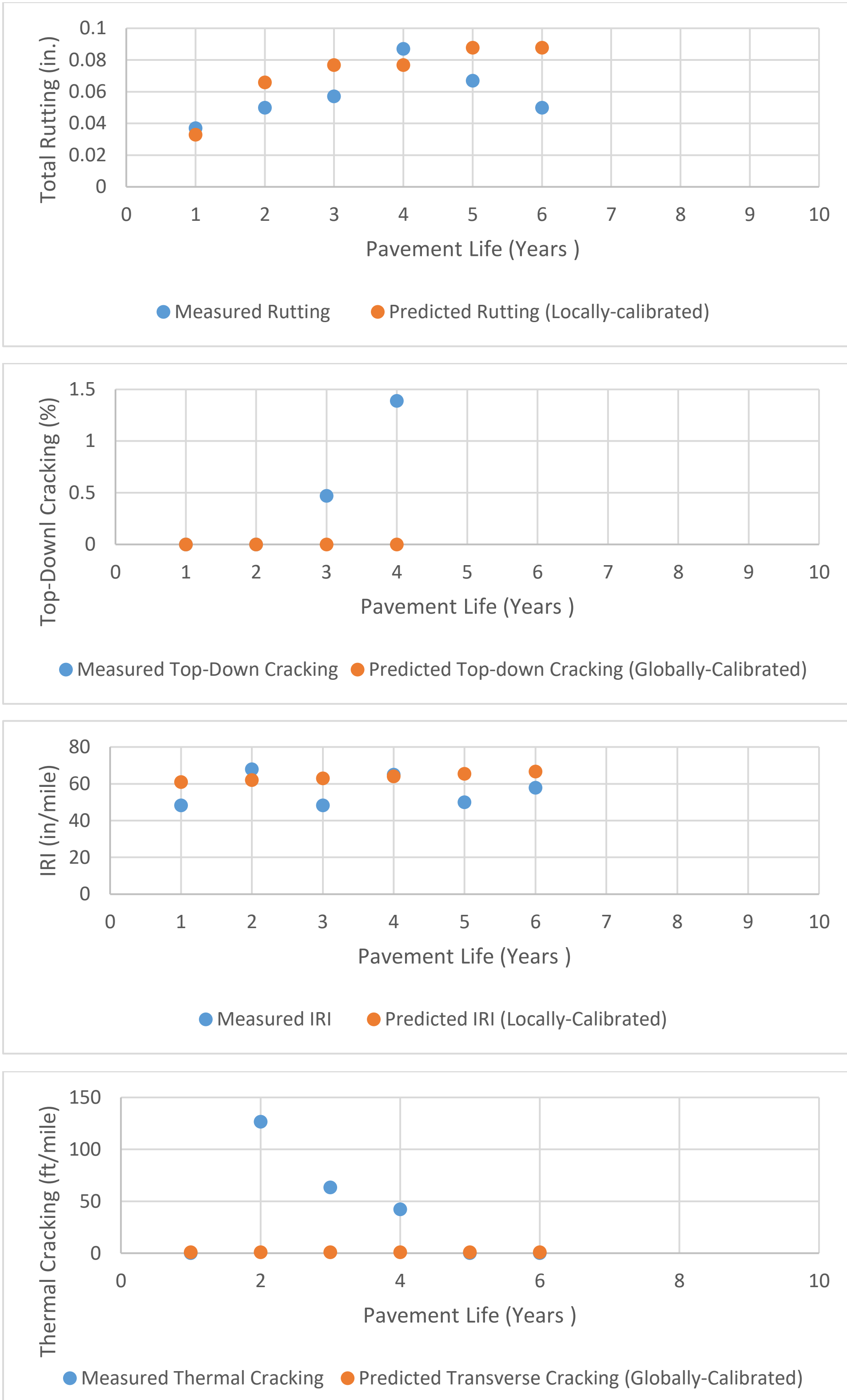

Figure B- 24. Measured and Predicted Performance Data for Project 095U0005600-EB

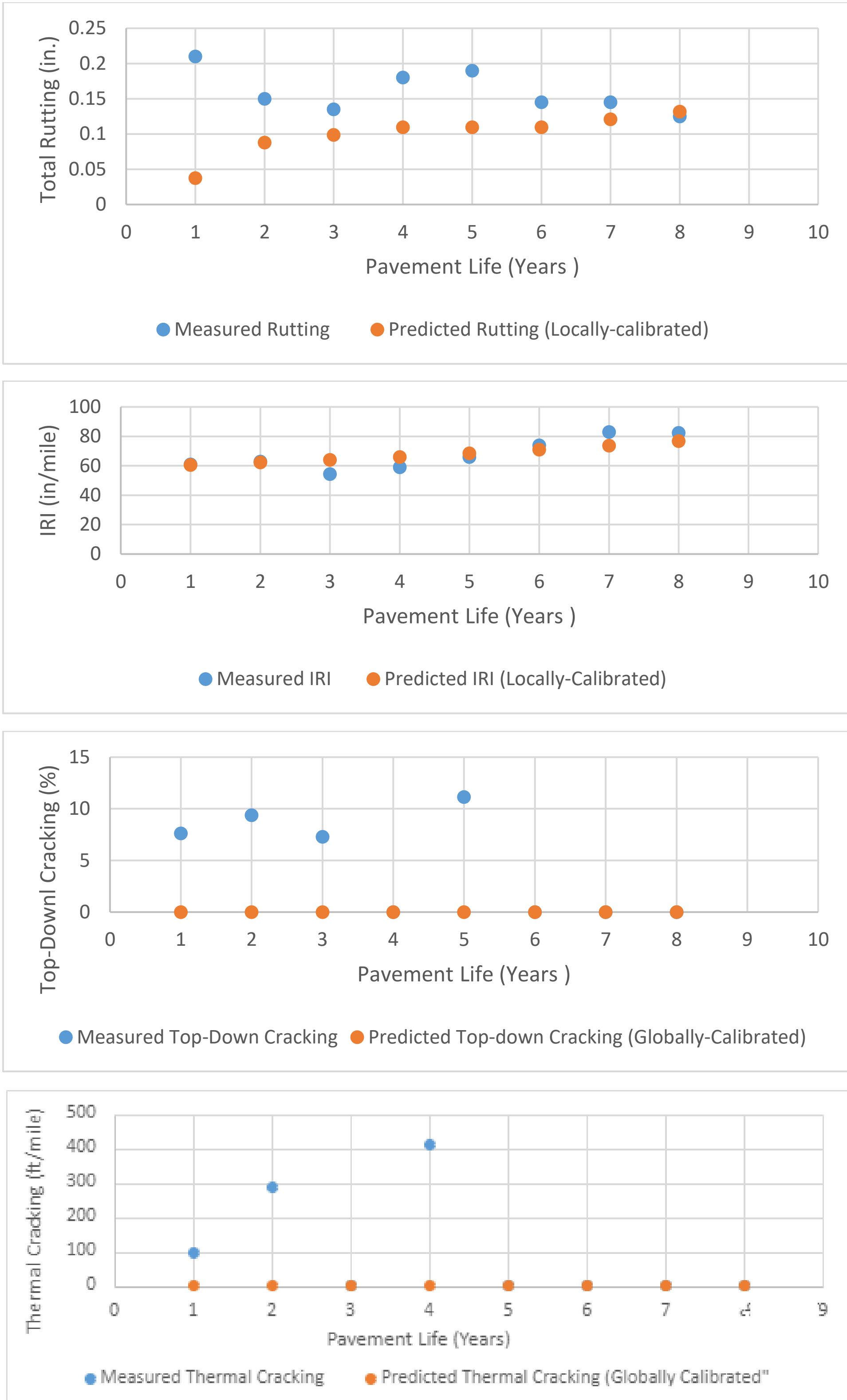

Figure B- 25. Measured and Predicted Performance Data for Project 103K0003900-NB